University of Zurich[UZH]

Analysis of surface structures and thermal distribution of Grenzgletscher ablation area with multispectral and thermal imagery

GEO 511 Master's Thesis

Author
Nicole Hanselmann
12-756-029

Supervised by
Dr. Martin Lüthi

Faculty representative
Prof. Dr. Andreas Vieli

04.10.2021
Department of Geography, University of Zurich

Abstract

Due to climate change, glaciers and ice sheets are increasingly melting. Many glaciers in polar and subpolar regions as well the Greenland and Antarctic ice sheet are polythermal. Which arises questions about how a polythermal glacier reacts, when a shift from a polythermal regime to a temperate regime occurs. The largest polythermal glacier in the Alps is the Grenzgletscher, where the ablation zone shows typical surface structures for cold ice. This makes the Grenzgletscher a perfect study site to study a polythermal glacier under warming conditions and then extrapolate the findings to the arctic and subarctic region.

The analysis of surface structures and thermal distribution at different locations on in the ablation zone of Grenzgletscher can be interpreted as studies under different climate conditions. By using multispectral and thermal imagery this thesis analyzed the surface of the ablation zone and tries to correlate the findings with the ice temperature. This analysis are important in understanding how a polythermal glacier adapts to warmer climate and what has to be considered in glaciological models.

Contents

List of Figures

List of Tables

1. Introduction

1.1 Climate change impacts on glaciers

Climate change is one of the most important topics at the time and it is popularly discussed in politics and economics. While most impacts of climate change are fuzzy, retreating glaciers are an impressive and straight visible sign of climate change. The IPCC (Intergovernmental Panel on Climate Change) lists glaciers as important indicators for climate change. This indicator examines the glaciers changes in length, area, volume and mass over time. Glacier mass balance is directly linked to atmospheric conditions (temperature, precipitation) and is therefore sensitive to changes in climate (IPCC, 2013). Retreating glaciers also have strong and lasting impacts on physical, biological and social system on regional and larger scale.

On regional to continental scale glaciers are often an important source of fresh water and influence the run-off seasonality, because glaciers store precipitation and release water in the melting season. The available water resources could shift from summer to spring, because of retreating glaciers, which has unfavorable effects on agriculture and irrigation in the lowlands (Hagg et al., 2013).

Glaciers only cover ~0.5% of the total land surface, without including the Antarctic and Greenland ice sheet, but they have a sea-level equivalent of 0.41m (IPCC, 2013). Therefore retreating glaciers are a main contributor of global sea-level rise in near future and could affect global ocean circulation, marine ecosystems and coastal regions.

Decline in snow cover and glaciers will amplify regional warming through snow and ice-albedo feedback effects (IPCC, 2013). The high albedo of snow and ice reflects most incoming radiation, while the lower albedo of rocks and sediment keeps part of the incoming radiation.

Retreating glaciers cause new landscape with leaving behind large amounts of unconsolidated sediments, rocks and new lakes, which increases the danger of natural hazards like landslides (Huggel et al., 2012), debris flows and glacial lake outburst floods (Worni et al., 2012). The enhanced sediment availability and erosion increase the chance of multiple kinds of natural hazards and needs to be considered in the management of former glacier covered regions. (Haeberli et al., 2021)

1.2 State of Knowledge

Glacier surface properties are important to understand and model glacier behavior. The division of glaciers into accumulation and ablation area (Benson, 1960) can give information about the glacier mass balance and is only the first step to classify glacier surface. The glacier surface and especially the albedo is important for energy balance (Cuffey and Patterson, 2010).

Data from monitored glaciers is crucial for modelling glaciers. But only a small and biased portion of glaciers is monitored in situ (Zemp et al., 2009) due to extensive logistical costs and bad accessibility (Pope and Rees, 2014.b) Therefore remote sensing offers the opportunity to monitor glaciers, globally and at low costs, with a high temporal repetition. Remote sensing (satellite imagery, aerophotogrammetry and drones) and GIS technologies increase the possibilities for analyzing and studying glaciers. Multispectral imagery is often the best tool for studying glacier surfaces (Pellikka & Rees, 2010). This technology provides information over a range of wavelengths, good spatial resolution, frequent repeat imaging, an extensive image archive, and often cost-free data access (Pope and Rees, 2014.a).

Multispectral remote sensing can be used to classify glacier surface into different classes / zones. The properties of these classes are used for a range of glaciological applications including mass balance measurements, glacial hydrology and melt modelling (Pope and Rees, 2014.a).

Thermal imagery is mainly used to differentiate between debris-covered ice and debris. Karimi et al. (2012) used the combination of optical and thermal remote sensing data to map a debris-covered glacier in Iran.

1.3 Study Area

The Gorner-/Grenzgletscher system is located at the south border of Switzerland in the Monte Rosa massif. It is the second largest glacier system in the Swiss Alps with a surface of almost 50 km^2 (Sugiyama et al., 2010) and known as the biggest polythermal glacier in the Alps. The highest accumulation basin of Grenzgletscher is Colle Gnifetti (4550 m a.s.l.) where cold firn is formed (Suter et al., 2001). Many ice-core drillings have been taken at the accumulation region at Colle Gnifetti (Oeschger et al., 1978, Smiraglia et al., 2000). The cold ice origin at Colle Gnifetti gets buried under temperate ice formed further down the accumulation zone. At the former confluence area of Gorner- and Grenzgletscher (2500 m a.s.l.) the buried cold ice appears on the surface and continues till the tongue (Eisen et al., 2009). This lower ablation area shows typical structures formed in cold ice, like supraglacial channels and lakes, and the cold ice area appears to be cleaner and brighter than the surrounding temperate ice (Ryser et al., 2013). The large supraglacial lakes and channels are reported for a long time (Renaud, 1936) and the polythermal structure makes

Grenzgletscher the subject of many scientific studies since the 1970 (Eisen et al., 2009). The good accessibility due to the Gornergrat Bahn, the near metrological station at Gornergrat, the long scientific history and especially the polythermal structure make the Gorner-/Grenzgletscher system a perfect study and test site to better understand the polythermal regimes of the Greenland and Antarctic ice sheet as well arctic and subarctic glaciers (Ryser et al., 2013).

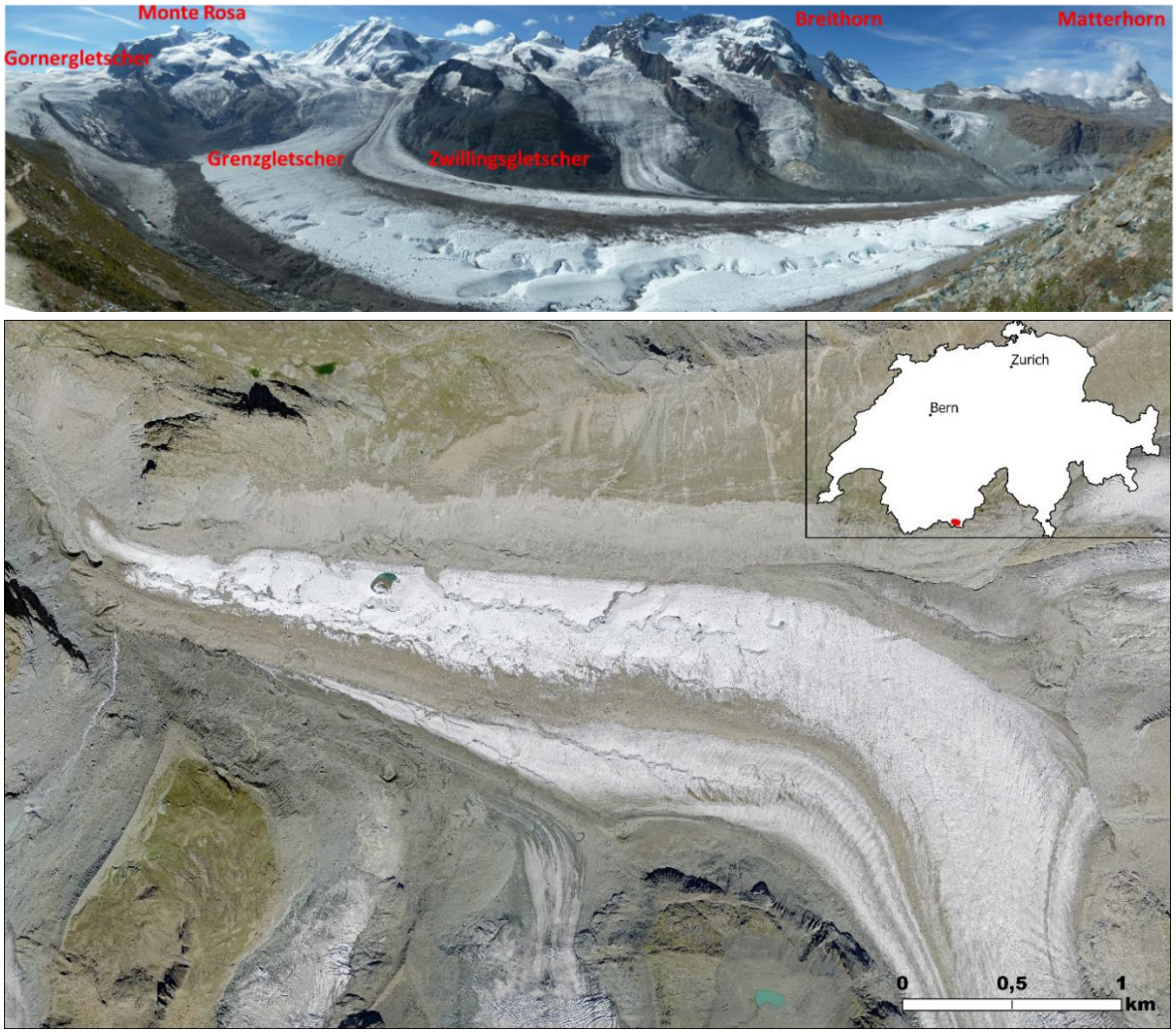

Figure 1: Overview of Gorner-/Grenzgletscher system (top): the accumulation zone in the Monte Rosa massif, the confluence area of Gorner- and Grenzgletscher and the cold ice ablation zone. Ablation zone and study area (bottom). Situation map with the localization of Grenzgletscher in Switzerland (small).

1.4 Research Questions

The lower ablation area of Grenzgletscher is covered a number of different surface structures. Especially deep meandering channels and supraglacial lakes and standing out and are typical for cold ice. This structures are often observed in the Arctic but rarely in the Alps. Since the thermal distribution of Grenzgletscher is well studied and recorded with different methods, the exact thermal regimes of many arctic glaciers is unknown. To examine the thermal distribution of a polythermal glacier, ground penetrating radar (Eisen, et al., 2009, Ryser et al., 2013) can be used to detect cold ice within the glacier. To get values for the ice temperature at different depth of the glacier, temperature must be measured in boreholes. Therefore the measurement of ice temperature and exact thermal regime is connected with intense fieldwork, which is makes this methods not suitable to monitor a glaciers worldwide. This raises the question, if it is possible to connect surface structures, which can be easily monitored by using remote sensing, with the ice temperature below. Based on the findings, that supraglacial water in channels and lakes are indicators for cold ice (Boon and Sharp, 2003) the followed questions were elaborated.

1. **Can typical surface structures for cold ice bodies give an indication about thermal changes in polythermal glaciers and how do they change under warming conditions?**

This first question analyses the distribution of typical surface structures like deep channels, supraglacial lakes, cryoconite holes and compares them with the ice temperature conditions based on Ryser et al. (2013).

2. **How does the north-south direction of deep meltwater channels influence their shape and features?**

Normally a deep channel tend to start in the middle of the glacier and flows outward (the north-south direction is based on the geographic position of the Grenzgletscher tongue). The channel is placed in similar climatic conditions from the start till the end of the channel, but the ice temperature changes form cold ice in the middle to temperate ice on the side of the glacier. This could give indications how a polythermal glacier will change when there is a regime shift to a temperate glacier under ongoing climate change.

3. **What do the “cold cracks” in the thermal images mean?**

This last question is based on the first views of the thermal datasets.

1.5 Content of this Master's Thesis

Chapter 1: A general overview about the impacts of climate change on glaciers and their consequences to humanity and the environment describe the greater context of this Master's Thesis. Followed by a short description on how remote sensing can be used to monitor glaciers and a short introduction of the study area. The research questions are presented.

Chapter 2: General theoretic background about glaciers, glacier surface, multispectral and thermal remote sensing and surface classifications based on spectral information.

Chapter 3: The study area is presented, with detailed information about the polythermal structure of Grenzgletscher.

Chapter 4 presents the data used in this thesis and the differences between the drones/cameras used on the three field campaigns. The processing of the data is explained, the methods used for the classification of the glacier surface and why this methods were chosen.

Chapter 5: The of the analysis of the multispectral and thermal datasets and the results of the classifications are presented.

Chapter 6: Discussion of the results and classifications and comparison with findings from literature. Difficulties and uncertainties are evaluated.

Chapter 7: Conclusion and outlook for possible future research.

2. Theoretical Background

2.1 Glaciers

Glaciers occur where climate conditions and topographic characteristics allow snow to accumulate over several years and transform into firn (snow that persists for at least one year) and finally to ice. Under the force of gravity, this ice flows downwards to elevations with higher temperatures where various processes of ablation (loss of snow and ice) dominate over accumulation (gain of snow and ice). (IPCC, 2013)

2.1.1 Thermal Regimes

Glacier can be divided into three thermal regimes, depending on the ice temperature.

Temperate glaciers: Temperate glaciers consists of ice at the pressure melting point, so water can coexist with glacier ice. In alpine regions temperate glaciers are most common.

Cold glaciers: In cold glaciers ice temperature is below the pressure melting point, no liquid water is contained in cold ice. Cold glaciers are frozen to the ground and exist mostly at high latitude or altitude. In the alps they only exist as small hanging glaciers in high-altitude.

Polythermal glaciers: Polythermal glaciers consist of both cold and temperate ice. Polythermal glaciers are common in the arctic and subarctic environment and also the Greenland and Antarctic ice sheets are polythermal (Ryser, 2014). In alpine regions, polythermal glaciers are restricted to high-elevation accumulation area, where cold ice could be formed (Eisen et al., 2009). Polythermal glaciers can have a wide range of thermal structures (Blatter and Hutter, 1991).

Temperature strongly influences ice viscosity, ice deformation patterns and mass flux (Blatter and Hutter, 1991), therefore knowing the thermal structure of a glacier is important and crucial for modeling. Cold ice influences the glacier hydrology, by limiting surface runoff to cracks and channels (Boon and Sharp, 2003).

2.1.2 Mass Balance

A glacier can be divided in two major area, the accumulation zone and the ablation zone. The accumulation zone describes where mass is gained and the ablation zone where mass is lost, the interplay of those two zones is the mass balance. The equilibrium line altitude (ELA) lies between the accumulation and ablation zones and the defines the line of net zero annual mass change (Cuffey

and Patterson, 2010). Snowfall is the main source of accumulation, but especially in polar regions and high altitude, where cold ice is formed, refreezing of liquid water is important. Ablation occurs mainly trough surface melting, calving or sublimation. Redistribution of snow by wind and avalanches can contribute to both accumulation and ablation (IPCC, 2013). A glacier with a positive mass balance is advancing, one with a negative one is retreating.

2.1.3 Glacier Surface

Glacier ice shows different kind of structures, which can be seen in field and also on remote sensing data. Depending on the level of dirt content and due to different physical characteristics of surface material, neighboring surface patches on a glacier show distinct wavelength-dependent reflection patterns (Hendriks et al., 2014, Pope and Rees, 2014.a).

Primary Stratification: Primary stratification is the result of the annual layering of the ice due to snowfall and melting processes. The dark layers represent summer ice, where pore spaces are filled with refrozen meltwater, and white layers of bubble-rich ice origin from winter snow. The layers are build parallel to the ice surface and deform with ice flow. The (Glasser and Gudmundsson, 2012).

Longitudinal surface structures: Longitudinal surface structures (or longitudinal foliation or flow stripes) develop in ice during ice flow and have planar or layered structure and are characterized by variations of ice crystals. They can be either be deformed primary stratification or during compressional and accelerating flow (Glasser and Gundmudsson, 2012).

Figure 2: Longitudinal surface structures on the ablation zone of Grenzgletscher.

Crevasses: Crevasses are cracks in the glacier formed when the elasticity threshold of ice is exceeded (Herzfeld et al., 2004). The ice structure fails in perpendicular direction to the maximal tensile

stress (Maisch and Jost, 2006). Crevasses occur frequently at the lateral margins of a glacier, at the snout or in regions of sudden change of the bed angle.

Medial moraine: Medial moraines normally form at the confluence area of two ice flows and get transported downwards the glacier.

Debris cover: Rock fall onto glaciers from the surrounding valley sides. The thickness of the debris cover is important for the glacier mass balance, since it can either increase melting or insulate the glacier ice.

Light-absorbing impurities: Light-absorbing impurities are all kind of impurities in snow and glacier ice, which affect the reflectance spectrum of the ice. Impurities get trough tree main processes into snow and ice. First, snowflakes forma around an ice nucei (Warren and Wiscombe, 1980). Second, they entrain particles in the air while falling (Magono et al., 1979), and third the impurity concentrations in snow are laying on the ground are further raised by fallout (Falconer and Hogan, 1971). Dirtier layer resulted by dry fallout and melting out of particles are formed every melt season (Warren and Wiscombe, 1980). This causes the primary stratification of the ice. Light-absorbing impurities often lower the albedo of glacier ice and therefore increase melting.

Cryoconite: Cryoconite is the aggregation of ice algae, organic matter and mineral particle (Takeuchi et al., 2001). The name comes from the Greek words kruos meaning ice and konis meaning dust (Gajda, 1958). Cryoconite can be spread out or trapped in cryoconite holes (Takeuchi et al., 2001). Cryoconite hole range from diameters of a few centimeters up to several meters. Cryoconite holes form with cryoconite flushing into depressions, the low albedo of cryoconite promotes then the melt into the ice (Takeuchi et al., 2001).

Cold ice and surface hydrology: Cold ice temperature is below the pressure melting point, which refreezes liquid water in cracks, which makes cold ice impermeable to water (Ryser et al., 2013, Boon and Sharp, 2003). This leads to surface runoff of meltwater and the transport of light-absorbing impurities and cryoconite into depressions (Ryser et al, 2013). This makes the cold ice cleaner and rises the albedo of the glacier (Takeuchi et al., 2001). Large supraglacial hydrological features, like deep meltwater channels and supraglacial ponds, indicate cold ice (Ryser et al., 2013).

2.2 Remote Sensing

Remote sensing offers the opportunity to collect more data of larger areas without taking in situ measurements. In general, remote sensing data covers larger areas than in situ measurements, but they should be calibrated and extend with in situ measurements. Especially the global coverage due

to satellites offers new perspectives in getting more insights on remote regions, as this is the case for glaciers in low populated mountainous environments and subarctic and arctic regions.

2.2.1 History

Remote sensing technologies can be used on a wide range of glaciological applications. Multispectral imagery is used for glacier maps and inventories, albedo calculation and monitoring (Dumont et al., 2012), distinguishing snow from cloud, identification of surface and basal crevasses, feature tracking and much more (Pope and Rees, 2014.a). Classification of surface classes like areas of wind gaze and sastrugi in Antarctica (Scambos et al., 2012), the temporal evolution of snow algae (Takeuchi, 2009) and dust (Painter, 2011) as well mapping debris cover on glaciers (Casey et al., 2012) were successfully done.

2.2.2 Multispectral remote sensing

Multispectral remote sensing can be obtained by drones up to satellites. Multispectral data is characterized by three resolution types. First, the spectral resolution gives information about the spectral range covered and the amount of bands used. Higher spectral resolution enables a finer classification of surface, by detecting more and smaller absorption bands. Second, the spatial resolution defines the ground area covered by one pixel. This can vary from cm (drones) to hundreds of meters (satellites). A finer spatial resolution enables the detection of smaller features, while a coarse spatial resolution is useful in providing values for global purposes. Third, the temporal resolution is given by the time passing in till the next picture of the same area is taken. The temporal resolution is important when working with satellite data. The multispectral data used for a specific task should be evaluated by these three types of resolution to fit the purpose.

2.2.3 Albedo and Spectral Profiles

The surface albedo of glaciers is important, because it affects the glacier mass balance and heat budget. A higher albedo reflects more solar radiation, while a lower albedo absorbs more solar radiation, resulting in more snow and ice melt. The surface albedo differs from glacier to glacier and also varies spatially and temporally (Klok et al., 2003). For the development of mass-balance models, the knowing of the spatial and temporal variation of the albedo is crucial. Major factors affecting glacier surface albedo are physical properties and impurities of snow and ice (Paterson, 1994). The

albedo of fresh snow is the highest and the snow albedo decreases with snowmelt and during transition to glacier.

Figure 3: Spectral reflectance curves for snow and ice in different formation stages. Bandwidths of Landsat TM bands 1-4 are given on top (Winter, 1993, fig.5).

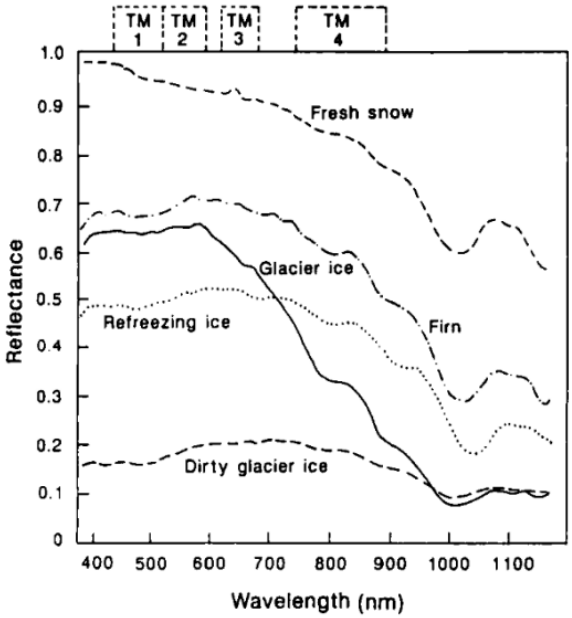

Spectral reflectance varies with physical properties of glacier surface and the quantity and optical characteristics of impurities (Warren and Wiscombe, 1980). Because there was no data set covering the full range of the Landsat VIR spectrum at high spectral resolution for an Arctic/temperate glacier Pope and Rees (2014.b) developed such a dataset based on in situ measurements. The spectra generated for this thesis will be compared to the spectra of Pope and Rees (2014.b).

Table 1: Description of the 7 surface classes measured on Midtre Lovéenbreen and 16 surface classes measured on Langjökull. See figures 4 and 5 for reflectance spectra. (Pope and Rees (2014.b), Table 1)

Glacier	Surface class	Description
Midtre Lovénbreen	Fine snow	Snow with grain size <2.5 mm
	Coarse snow	Snow with grain size >2.5 mm
	Slush	Saturated snow of any grain size
	'Dry' ice	Glacier ice with a friable surface and minimal liquid water content
	Dry semi-saturated ice	Glacier ice with a visible but small amount of liquid water on the surface
	Wet semi-saturated ice	Glacier ice with a significant liquid water content on the surface
	Saturated ice	Glacier ice which is completely saturated with water on the surface, either streaming or very shallow ponding
Langjökull	New drifted snow 1, 2, 3, 4	Snow which fell during the period of data collection, redistributed by wind
	Ashy snow 1 & 2	Snow from the preceding summer with a dusting of volcanic ash which had not ablated into large pits
	Ashy snow pit side	Snow from the preceding summer on the side of the large pits caused by differential melting resulting from volcanic ash deposition with a moderate ash concentration
	Ashy snow pit bottom	Snow at the bottom of ash-induced melt pits (up to 2 m deep) with the highest ash concentration observed
	White ice 1 & 2	Glacier ice with a friable surface, minimal liquid water content, and no apparent ash
	Wet ashy ice 1 & 2	Glacier ice with some liquid water content and apparent volcanic ash
	Debris ice	Glacier ice with some non-ash debris
	Very debris ice	Glacier ice with the majority of the surface covered by non-ash debris
	Stream ice debris 1 & 2	Glacier ice overlain with very shallow flowing melt water and accumulated debris

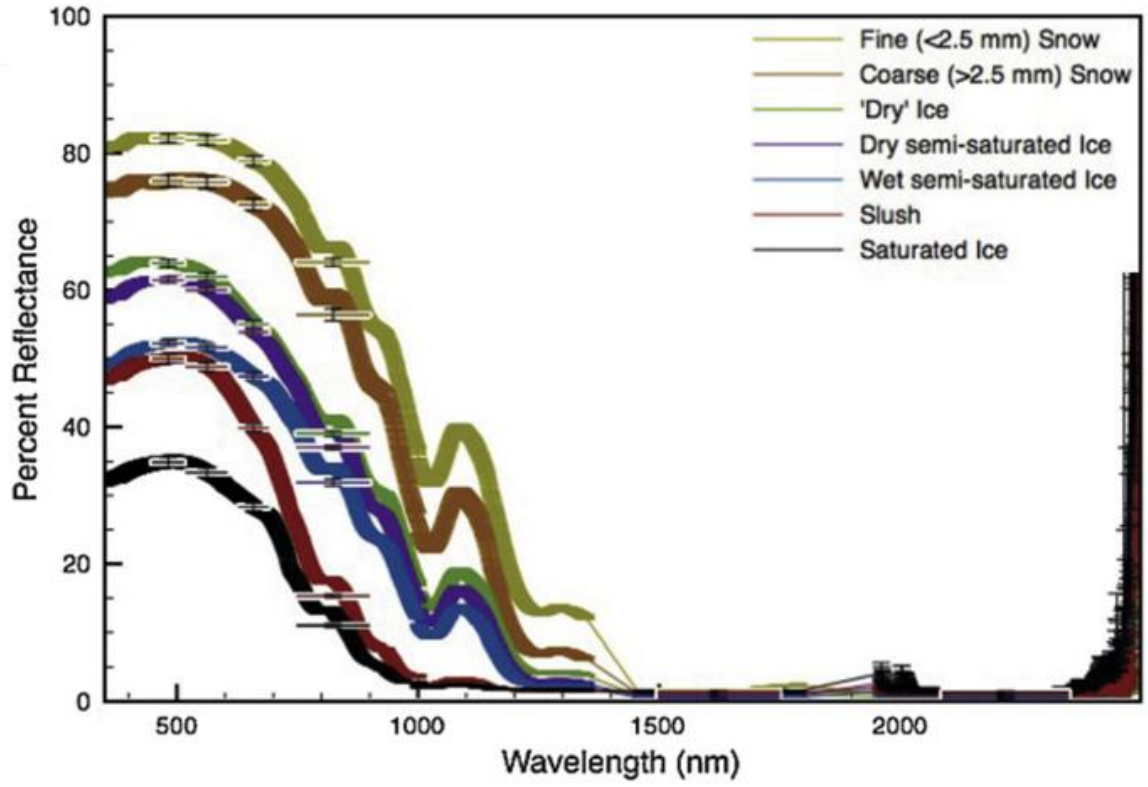

Figure 4: In situ reflectance spectrum from Midtre Lovénbreen. (Pope and Rees (2014.b), figure3)

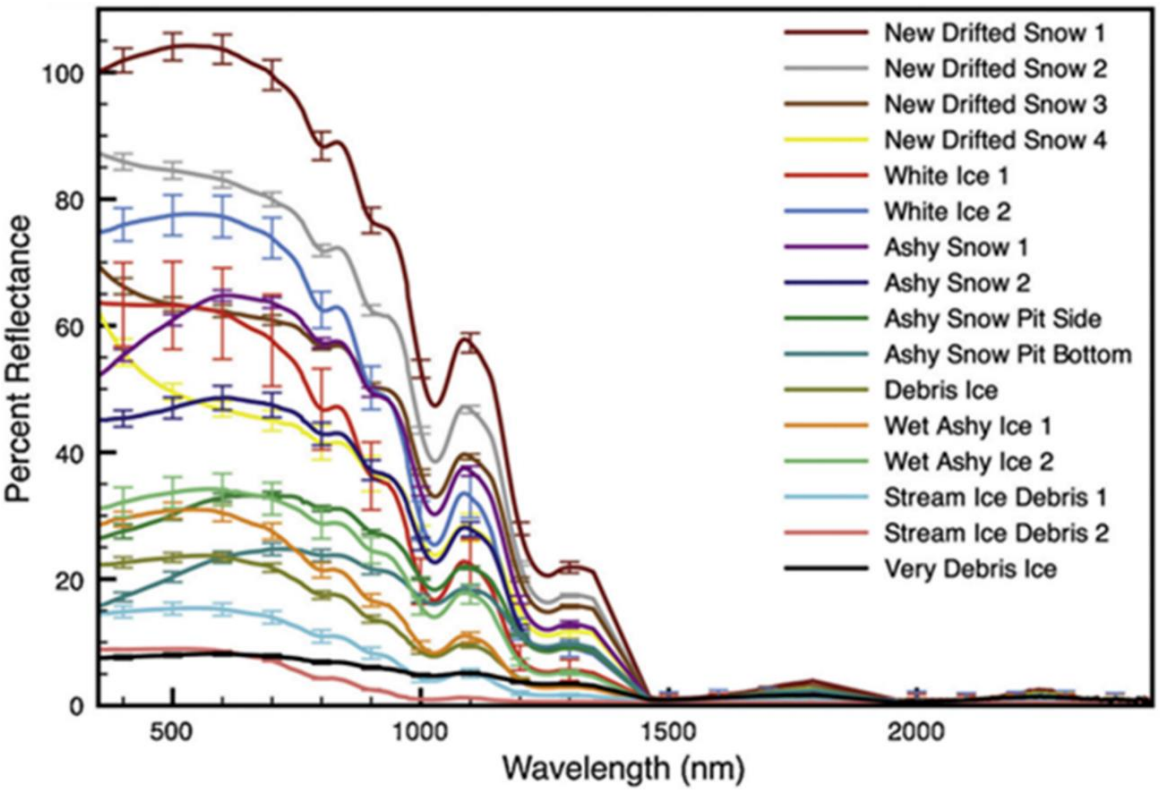

Figure 5: In situ reflectance spectrum from Langjökull. (Pope and Rees (2014.b), figure 3)

2.2.4 Surface Classification

Classification, the process that takes quantitative information from every pixel and places each into one group of discrete categories, is crucial for image interpretation (Pope and Rees, 2014.a). To identify surface classes on multispectral data many different techniques have been applied. The automated classification of glacier extend is largely solved, except for debris-covered areas (Paul et al., 2013). Unsupervised classifications, like ISODATA and k-means) are successfully used in classifying glacier facies (Pope and Rees, 2014.a). Unsupervised classifications is reproducible and the detection of subtle features within datasets is possible. While supervised classification depends on the visual classification depending on knowledge and experience of the person doing the classification or on spectral databases, which must be representative for the study area.

There is no general definition of good or bad data based on the spatial resolution, it depends on the particular application the data is used for. In coarse imagery pixels are representing a mixture of classes, while a fine spatial resolution is more likely to contain pure classes. Many studies have been done about the comparison of classification results based on different spatial resolutions, for example on glacier surface (Pope and Rees, 2014.a/b). However a finer spatial resolution does not necessarily result in better classification results, coarser spatial resolution smooths spatial inhomogeneity within classes. Pope and Rees (2014.a) summarized other studies about glacier classification based on different spatial resolution and concluded, that there is no significant difference in measured glacier area using imagery at 60 m resolution of finer. They also mentioned that albedo variations is smaller than 30m pixels, but because albedo can vary within facies, which are not necessarily vary on the same scale. This can influence the surface classification with finer spatial resolution than 30 m, meaning that a surface class can be split up because of different albedo values.

Snow and ice reflectance are heavily wavelength-dependent (Warren and Wiscombe, 1980). Near infrared (nir ~700-1400nm) is seen as containing quantitive information about snow and ice surfaces (Kokhanovsky and Zege, 2004). Pope and Rees (2014.a) concluded that sensors with enhanced capabilities in the NIR will be able to classify glacier surface better than their counterparts.

2.2.5 Thermal Imagery

With the advent of thermal infrared satellite imaging in the 1960s the acquisition of large-scale spatiotemporal variations of surface temperature patterns was possible (Wu et al., 2019). However the accuracy of land surface temperature is still a great challenge (Wu et al., 2019), because of the multiple influence of surrounding area onto the temperature measured with remote sensing.

Therefore temperature measurements in boreholes is still widely used in glaciology. Ground-penetrating radar has been used to identify cold ice and successfully used for detecting thermal regimes within glaciers (Ryser et al., 2013).

The following paragraph about supraglacial debris covered glaciers is based on Karimi et al. (2012). Supraglacial debris covers on the glacier surface and on its surrounding introduce high uncertainties in glacier area mapping, because of same reflectance characteristics. There are three method categories to overcome this problem. The geomorphometric-based methods attempt to combine characteristic features of debris cover areas, based on DEM parameters like slope, aspect and curvature (Bolch and Kamp (2006) and Paul et al. (2004)). This method highly depends on the quality of the DEM. Therefore radar imagery-based methods have been developed. Thermal-based methods are based on the lower temperature of debris-covered glaciers from periglacial debris outside the glaciers margins (Ranzi et al., 2004). This thermal based attempt is effective when the debris cover does not exceed a thickness of 40-50 cm.

3. Study Area

3.1 Gorner- / Grenzgletscher System

The Gorner-/Grenzgletscher system involves five tributaries (Gornergletscher, Grenzgletscher, Zwillingsgletscher, Schwärzgletscher and Breithorngletscher), the entire system covers an area of almost 50 km^2 and ranges from 2200 m to 4634 m a.s.l., the central flow line is ~12 km long (Benoit et al., 2018). Since the 1970s the Gorner-/Grenzgletscher system is widely studied, because of its size, thermal regime, accessibility and glacier dammed lake (Sugiyama et al., 2010). The long history of glaciological studies show, that the Gorner-/Grenzgletscher system was stable from 1930s to the early 1980s (Benoit et al., 2018) and since then significantly dropped (Huss et al., 2012). Warming of local climate can be associated with a rise of the Equilibrium Line Altitude (ELA) to nowadays around 3300 m a.s.l. according to studies at the neighboring Findelengletscher (Sold et al., 2016).

In the accumulation zone at Colle Gnifetti (4550 m a.s.l.) ice temperatures between -14.1 °C and –12.5 °C throughout an ice column were measured (Haeberli and Funk, 1991; Lüthi and Funk, 2001).

3.2 Polythermal Structures of Ablation Area

The cold ice of Grenzgletscher originates in the accumulation region at Colle Gniffetti, where the glacier is cold and frozen to bed (Haeberli and Funk, 1991; Lüthi and Funk, 2001). Further down the accumulation region and also on the upper ablation region, including the equilibrium line, temperate firn and ice are present as surface layer on top of a cold layer of ice (Eisen et al., 2009). The exact position of where strain heating and geothermal heat flux cause the onset of the melting at base is unknown (Eisen et al., 2009). This implements the beginning of a temperate layer at the bed. With ongoing melting further down the ablation area the temperate surface layer gets completely melted and the cold ice reaches the surface again. Apart from the cold ice formed in high altitude the lateral parts of Grenzgletscher including the medial moraines are temperate (Eisen et al., 2009).

The following description (rest of chapter 3.2) of the ice temperature distribution and the cold ice layer in the ablation zone of Genzgletscher is completely based on the study of Ryser et al. (2013), where the cold ice in the ablation zone was analyzed.

The cold ice within Grenzgletscher is localized in a central flow band of 400m width, while the surrounding ice and the bottom layer is temperate, The coldest temperature in the cold layer can be found at 60 – 80 m depth. The ice temperature gradually increases along the flow line in downstream direction. Measurements from boreholes indicate a thinning cold core and a thickening temperate basal layer along the flow line. The ice under the medial moraine is temperate, because it was near the valley walls further upstream. The cold ice temperature profiles show typical shapes for a regime

dominated by heat advection, like this is the case for fast flowing polar glaciers. The conversion of potential energy to heat, caused by the downflow of the glacier, has the potential of raising the temperature by 9.5 K during a 2000 m drop. Since the ice in upper half of ice body barley deforms, the energy is released at the bed and the temperate layer forms. Melted ice at the bottom is a continuous source of subglacial meltwater.

Cold ice has higher viscosity than temperate ice, which affects the glacier dynamics. In the central part of Grenzgletscher cold ice occupies between 70 – 90% of the ice thickness, therefore the flow pattern in the whole confluence area is affected. This is especially important for ice flow models.

Cold ice is impermeable to meltwater and leads to supraglacial runoff in cracks or channels. Not flowing water within cold ice refreezes within days. Surface morphological features can form because of the impermeability of cold ice. On Grenzgletscher lakes of more than 20 m diameter, meltwater streams flow through deep (10 – 30 m), meandering canyons have formed and they persist for many years. This kind of surface morphology is unique in the Alps, but often observed in Arctic polythermal glaciers. This deep channels and supraglacial lakes only exist in the cold ice of Grenzgletscher and are absent in the temperate ice. The locations of persistent, deeply incised hydrological features at the glacier surface coincide with the areas where cold ice was mapped. In contrast the density of moulins is high in temperate ice, while only one cold ice area with moulins. This area is located in the crevassed zone, which is caused by the extensional stresses as the ice flow changes direction. Few moulins can be found in the center of the cold is further downstream from the crevassed zone. Most likely the were formed in the crevassed zone and got advected. Those moulins must carry large meltwater fluxes, so that they do not refreeze during winter.

In the past an ice marginal lake (Gornersee) was formed every summer in the confluence of Gorner- and Grenzgletscher. The lake drained between 4 and 6 x 10^6 m^3 water within several days during an outburst flood in midsummer. In 2004 and 2008 different drainage has been observed, subglacial, englacial through a big channel, and superficial through a progressively incised gorge. However this lake does no longer form.

3.3 Study Area on the lower Ablation Area

The study area of this thesis is located on the lower ablation area of Grenzgletscher. It spans a range from 2250 m to 2500 m a.s.l. and has a length of 4 km. The area is relatively flat and characterized by deep meltwater channels and is partially debris covered. The study area varies for each drone dataset, this is mainly because the data was acquired by different people and not mentioned to be analyzed together. This datasets were collected on other fieldtrips and have not been used. The study

area for the APEX flight in 2016 is covering the whole lower ablation area starting approximately there, where the ablation area becomes flat, downwards to the snout. The datasets from 2018 cover the area from the former confluence zone downwards to the large supraglacial lake. The extent shown in figure 6 represents the area covered by the thermal dataset, the RGB dataset covers a similar area as the 2019 morning 3 flight. The data from 2016 and 2018 was collected in September on midday time. The flights from 2019 cover areas with deep meltwater channels in the middle of the lower ablation area. The area shown in figure 6 represent the extend of the RGB, VIS and NIR datasets. The thermal datasets lie within these areas, but only cover parts of it. The datasets were simultaneously acquired, since the drone was equipped with all cameras at the same time. There was one fight carried out on late evening (9 pm, local time) and three flights in the early morning (6 am). The reason for choosing this times is unknown to the author, but a midday time would be more suitable for multispectral imagery. Because multispectral imagery uses passive sensors, which depend on sunlight as a light source.

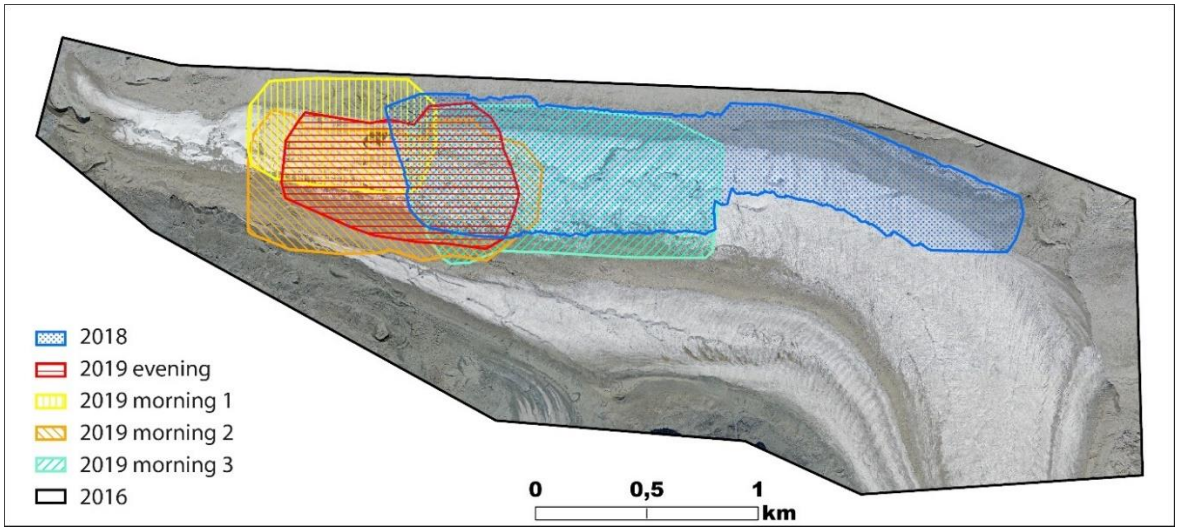

Figure 6: Area covered by different drone flights on aerial photo of SwissImage (swisstopo, 2021: Acquisition year: 2015). The APEX flight is covering the whole lower ablation area of Grenzgletscher with hyperspectral data acquired in 2016. The flight from 2018 (blue) was only recording thermal data. While all the flights from 2019 recorded RGB, VIS, NIR and thermal data. Therefore the comparison of multispectral data is only available between observations from 2016 and 2019, and for thermal data between 2018 and 2019.

4. Material and Methods

4.1 Drone data

For this thesis drone data from field campaigns in 2016, 2018 and 2019 is used. These three field campaigns where carried out by different people and with different drone set ups. While the data from the campaigns in 2016 and 2018 were already fully processed and usable, the data from 2019 was only partly processed. The main data collection for this thesis is the multispectral and thermal data collected in 2019. The other two campaigns collected either hyperspectral data (2016) or thermal and RGB data (2018) but not both (see table 2).

4.1.1 Campaign July 2019

The main dataset for this thesis was acquired on two days in July 2019, during that field campaign 4 drone flights were made. There was one flight taken in the evening after 9pm and three flights the next morning starting before 6am. All the flights took place in the lower ablation zone of Grenzgletscher starting approximately from 800m till 3000m away from the tongue. The different flights covered partly overlapping areas (see figure 3). The drone used in this campaign had four cameras on (RGB, VIS, NIR and thermal). The ground resolution of the RGB image is 0.1 m, while the thermal image has 0.4 m. The instrument for the visible spectrum has 16 bands recording a spectral range from 470 nm to 630 nm (Photonfocus, a) with a ground resolution of 0.6 m. The near infrared instrument has 25 bands with a spectral range from 600 nm to 975 (Photonfocus, b) nm and recorded a ground resolution of 0.75 m.

4.1.2 Campaign September 2018

On a fieldtrip in 2018 a drone flight over the lower ablation area of Grenzgletscher was made. The drone covered an area starting slightly above the large supraglacial lake (approximately 1.5km from the end of the tongue till the former confluence area of Gorner- and Grenzgletscher. The drone was equipped with a thermal radiometric infrared and a RGB instrument. The thermal dataset has a ground resolution of 0.25m and the RGB dataset 0.1m.

4.1.3 Campaign APEX September 2016

APEX (Airborne Prism Experiment) is an advanced scientific instrument for the European remote sensing community, recording hyperspectral data in approximately 300 bands in the wavelength

between 400 nm and 2500 nm and at a spatial ground resolution of 2 m to 5 m (APEX, 2021). APEX is based on the detection of many narrow, contiguous spectral bands and has the possibility for more precise identification of surface materials (APEX, 2021) than the instruments used on the field campaigns in 2018 and 2019.

For this thesis data from the APEX campaign "Findelen 2016" is used. In this campaign 6 flights in the region of Findelengletscher, a neighboring glacier of Grenzgletscher, were made and flight line 5 is covering perfectly the whole ablation area of Grenzgletscher. The data was recorded on the 06. September 2016 after midday with a ground resolution of 2 m and 284 bands covering a range from 409 nm to 2437 nm.

Since this dataset is covering the whole study area as well a wide spectral range it is used as the reference dataset for the Grenzgletscher in the analysis.

Table 2: Instrument description of the different drones used in the field campaigns.

Campaign	Instrument	Spectral Range	Number of Bands	Ground Resolution	Acquisition
2019	Blackfly	RGB	3	0.12 m	Evening
	Photonfocus	VIS 470 – 630 nm	16	0.60 m	Morning
	Photonfocus	NIR 600 – 975 nm	25	0.75 m	
	Thermal		1	0.39 m	
2018	senseFly	RGB	3	0.10 m	Afternoon
	Thermal		1	0.25 m	
2016	APEX	VNIR 380 – 970 nm SWIR 940 – 2500 nm	284	2 m	Midday

4.2 Data processing

The data acquired by the different field campaigns was already existing at the start of this thesis and not collected by the author. While the data from 2016 and 2018 was fully processed and directly usable the data from 2019 was only partly processed. Section 4.2.1 describes therefore only the processing of the 2019 datasets.

4.2.1 Image processing

The datasets from the field campaign 2019 were a combination of processed and raw data. The dataset contained directly usable RGB and thermal datasets as well a DEM of each flight. The VIS and NIR data was only partly processed and contained thousands of single images.

To get from the single images to mosaic images, which covered the whole flight area the software Pix4Dmapper was used. With the function create 4D maps the data of the different flights and cameras could be automatically processed. As input all pictures from one camera, for example from the vis camera, were taken together with the geolocation data of the drone for each picture. Then the program performed time intense calculations based on three steps (initial processing, point cloud and mesh, DSM and orthomosaic). The created orthomosaics showed the whole flight of the drone from starting point to landing. Since this created datasets contained unclear pixels at the edge of the mosaics, they were masked by hand so that only clear pixels were left.

4.2.2 Image classification

The processing and analyzing of the data was made with the GIS software ArcGIS and QGis, both software provide similar functions with slightly differences in the data processing.

The first step of data processing was to mask the datasets of the same flights to the same extend. This was done by using the 'clip raster' tool to cut the larger datasets to the extent of hand-defined mask. The extent of each flight is shown in figure 3 (chapter 3.3).

Classification Wizard (ArcGIS)

One of the goals of this thesis was to make a surface classification based on the multispectral datasets. Since the datasets have different amount of bands with different recorded wavelength, separate classifications for the datasets from 2018 and 2019 (VIS, NIR and combination of both) and also each flight was made. The first attempt was to create reference classes for different datasets (VIS, NIR and combination) based on one of the 2019 flights and use them for classify the other 2019 flights. For this purpose the ArcGIS tool Classification Wizard is perfect, because it leads through the whole classification process and can also produce a reference class dataset.

To get a basis idea about the distribution of different surface classes on the ablation area of Grenzgletscher, the hyperspectral dataset from 2018, which covers the whole area, classified with the Classification Wizard. Because there was no reference dataset for glacier ice classes available an unsupervised pixel-based classification was chosen. The Classification Wizard then performed an ISO Cluster classification, where pixel where put in the same class when they have similar attributes. This method produces satisfying results for the two datasets, but then however the tool started to fail and not process any further datasets, even crash the whole ArcGIS. Because this problem could not be fixed the whole classification procedure was carried out with the classification tool "unsupervised ISO-Cluster-Classification".

Unsupervised ISO-Cluster-Classification (ArcGIS)

The unsupervised ISO-Cluster-Classification is a classifier based on the maximum-likelihood-method, this means this classifier works similar to the classification wizard. The main difference is, that the number of classes need to be defined as input. Based on the experience with the classification wizard the amount of 7 classes were chosen. The aim behind 7 classes is, that the glacier ice gets divided into 3 or 4 classes. When less classes are chosen mainly the ice classes have been aggregated and with more classes, they mostly represented different moraine material. On the other side 7 classes seem to create a meaningful amount of classes, while more classes tend to overload the output images.

Raster Layer Zonal Statistics (QGIS)

Since ArcGIS failed to produce spectral signature of the classes generated with the unsupervised ISO-cluster-classification, the spectral signature information was generated in ArcGIS. As example the original 2016 apex dataset with all the band information was taken as input together with the file, which represents the 7 classes produced for that dataset. Then the zonal statistics were calculated, by taking the values of each pixel within a class and calculate the statistics. However this tool calculated the statistics only for one band and created a table of the results. By running this tool as batch process, tables for each band were calculated, which means for the apex dataset a total of 284 tables. Therefore the zonal statistics tool was run within a python code, that the outcome was only one table where the means for each band and class were provided. From this means the spectral signature curves were built with excel.

For the flights of 2019 the spectral signature was only calculated for the combination of the VIS and NIR datasets, with the classification for this combination.

5. Results

5.1 Surface Classification

This section is presenting the surface classification results of the multispectral datasets together with the spectral profiles for each dataset.

5.1.1 General overview of classification results

2019 Evening Flight

The evening flight was classified in 4 ice classes and 3 moraine classes. The brightest ice classes are placed in the middle of the tongue, the classes towards the valley walls and of the medial moraine contain darker ice. The VIS and NIR classifications (figures 17 and 18) positioned the normal ice class in the middle flanked by the bright ice class. While the combination of the NIR and VIS channels classified more pixels within bright ice and placed this class more on the center. The classifier could not recognize the supraglacial lakes as water, even when the RGB image (see figure 28) does show blue water. In all three classifications the water was added to the darkest moraine class. Large meandering channels can be distinguished from the surrounding ice, because they were assigned different classes. Sediments transported and deposited in the channels are classified within the moraine classes, as well as large supraglacial cryoconite holes or debris and larger rocks on the glacier.

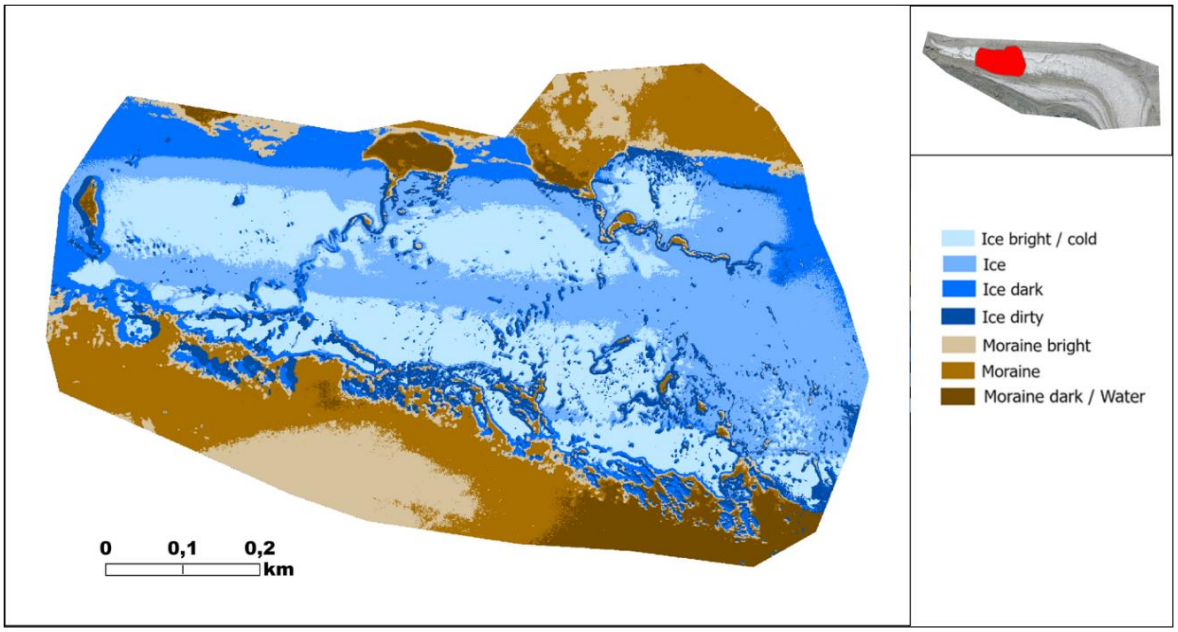

Figure 7: Classification for the evening flight 2019 based on the combination of the VIS and NIR datasets.

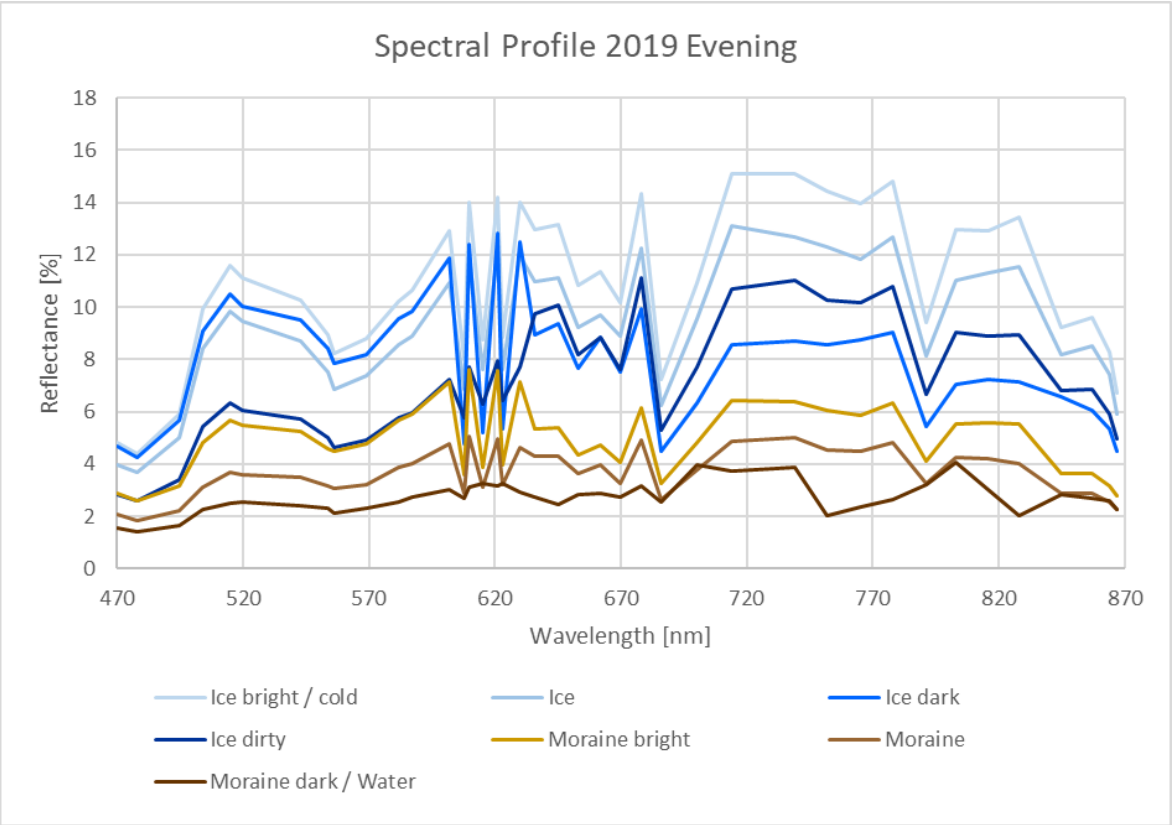

Figure 8: Spectral profiles based on the combined VIS and NIR classification for the evening flight 2019.

The spectral profile for the evening flight confirms the differentiation between the ice classes and the moraine classes. The bare ice classes Ice bright /cold, Ice and Ice dark have higher reflectance over the whole measured spectrum than the moraine classes. The dirty ice class has reflectance values similar to the bright moraine at wavelength below 620 nm, for wavelength above the reflectance is much higher, even above the dark ice. This class seems to be influenced by the offset effect because there is a shift in the spectral reflectance profile from moraine class behavior to ice class behavior at 600 nm, this is exactly where the wavelength covered by the VIS and NIR cameras overlie. The shift can also be visible interpreted as visible at the supraglacial lake, which is placed the closest to the snout). On the left side of the lake the ice is classified as dirty ice, while on the other side as dark ice. The dirty ice there represents is mapped as lake in the VIS band and as ice in the NIR bands, the opposite is the case on the other side. Where the dark ice class includes ice from the VIS bands and lake from the NIR bands.

2019 Morning Flight 1

The first morning flight was classified with 3 ice classes, 2 ice / moraine mixture classes and 2 moraine classes for the VIS and combination image. The NIR classification resulted in 4 ice classes and 3 moraine classes. Apart from the upper third of the classified image the ice classes seem to be a good representation of the glacier ice for all three classifiers. The mixture classes, for the VIS and

combination image, contain closer to the medial moraine much brighter ice than close to the glacier margin towards the valley wall. The NIR image classifier classifies the mixture classes from VIS and combination, as dark ice (close to the medial moraine) or bright moraine material (close to the valley wall).

All classifiers classified the upper half of the valley wall within the ice classes, which is clearly wrong, because there is no ice (see figures 19 and 20).

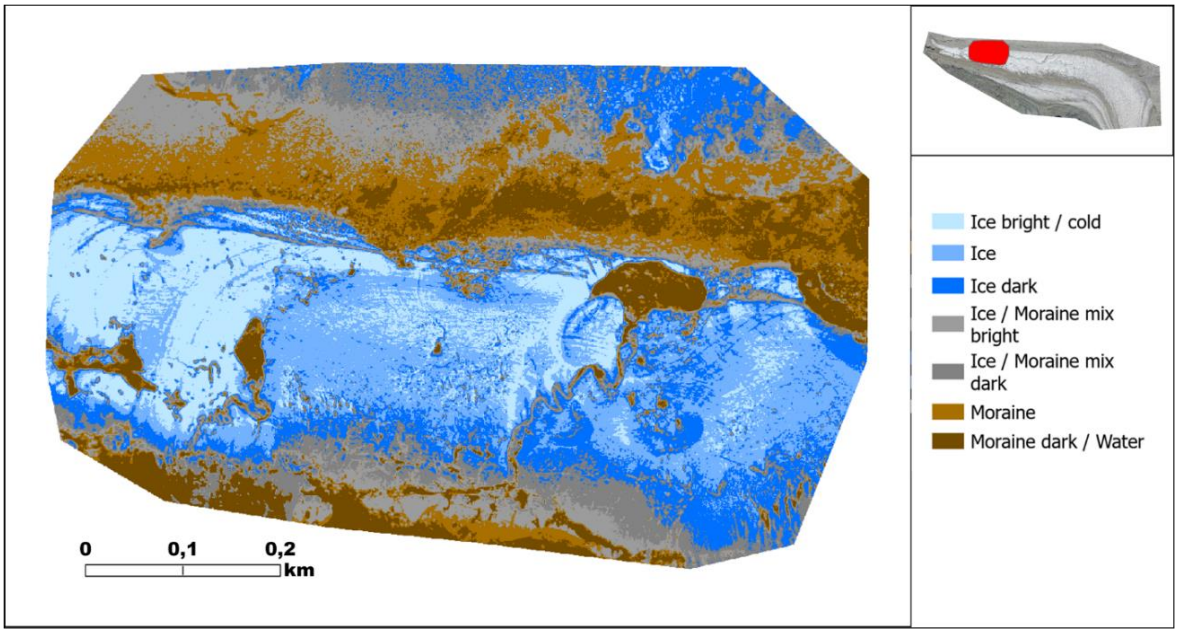

Figure 9: Classification for the first morning flight 2019 based on the combination of the VIS and NIR datasets.

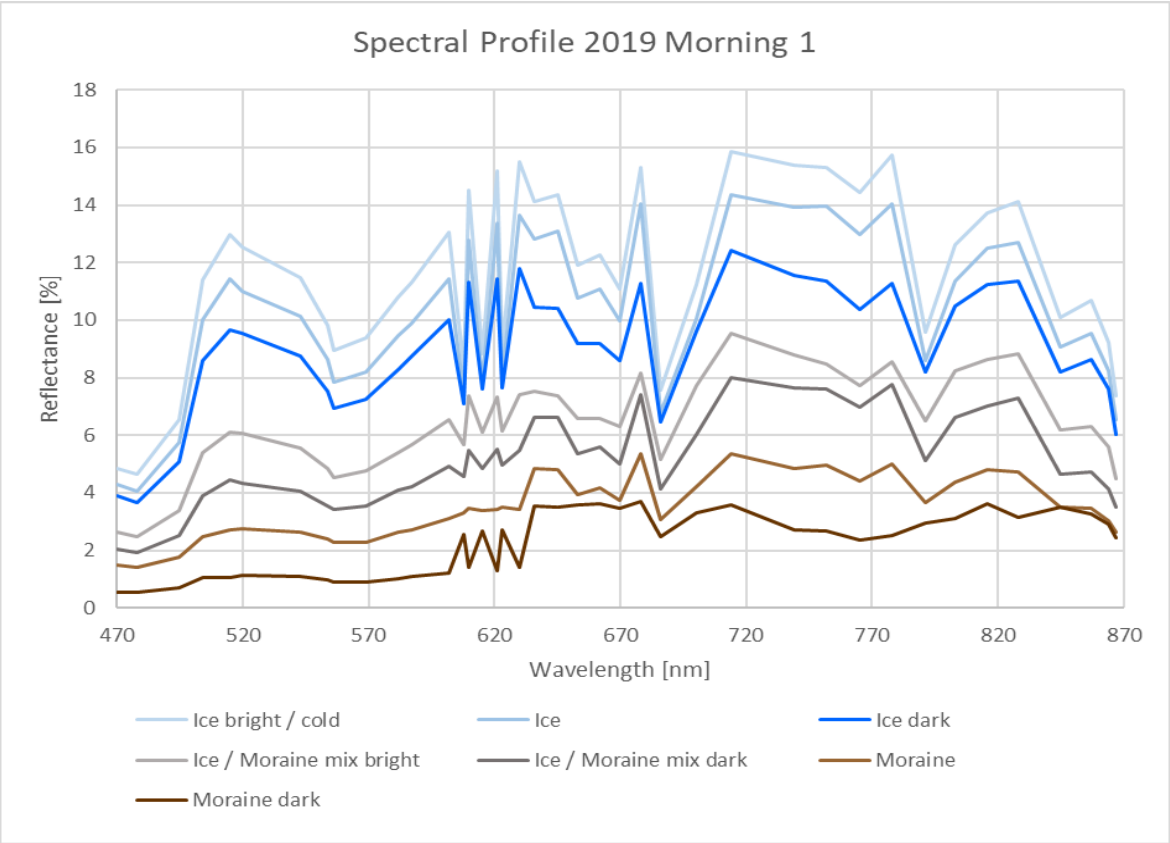

Figure 10: Spectral profiles based on the combined VIS and NIR classification for the first morning flight 2019.

The reflectance curve of the first morning flight shows similar spectral profiles behavior for all classes over the entire spectrum, but at different levels of reflectance. The mixture classes behave as expected and are placed in between moraine and ice classes.

2019 Morning Flight 2

The second morning flight contains also 2 mix classes, 2 moraine classes and 3 ice classes. The cold ice classes are meaningfully distributed with brighter ice closer to the medial moraine than the valley side. On the this area of Grenzgletscher are many hydrological features like meandering channels, supraglacial ponds and cryoconite holes. All three classifiers classified those features within the moraine categories, therefore they can easily be distinguished from the surrounding ice classes. The two mix classes are located on the medial moraine at the site of Zwillingsgletscher. This is mostly an area with a thin debris cover and visible ice features within the debris. But also regions at the valley side of Grenzgletscher are identified as ice debris mixture, even when they are clearly bare ice in the RGB image (see figure 32).

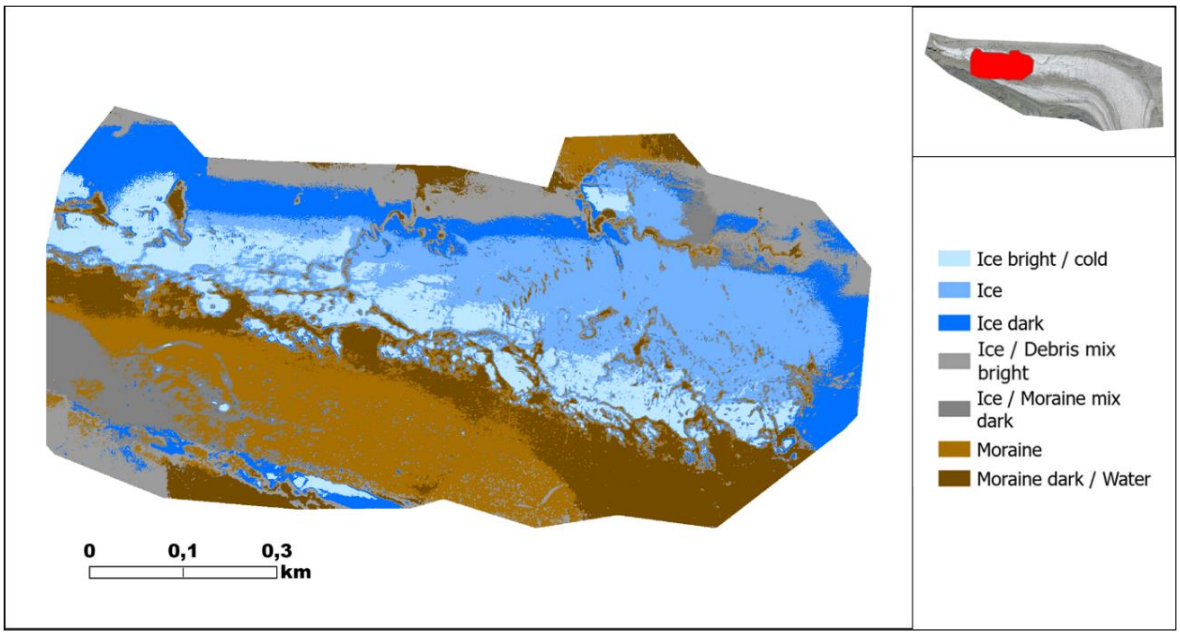

Figure 11: Classification for the second morning flight 2019 based on the combination of the VIS and NIR datasets.

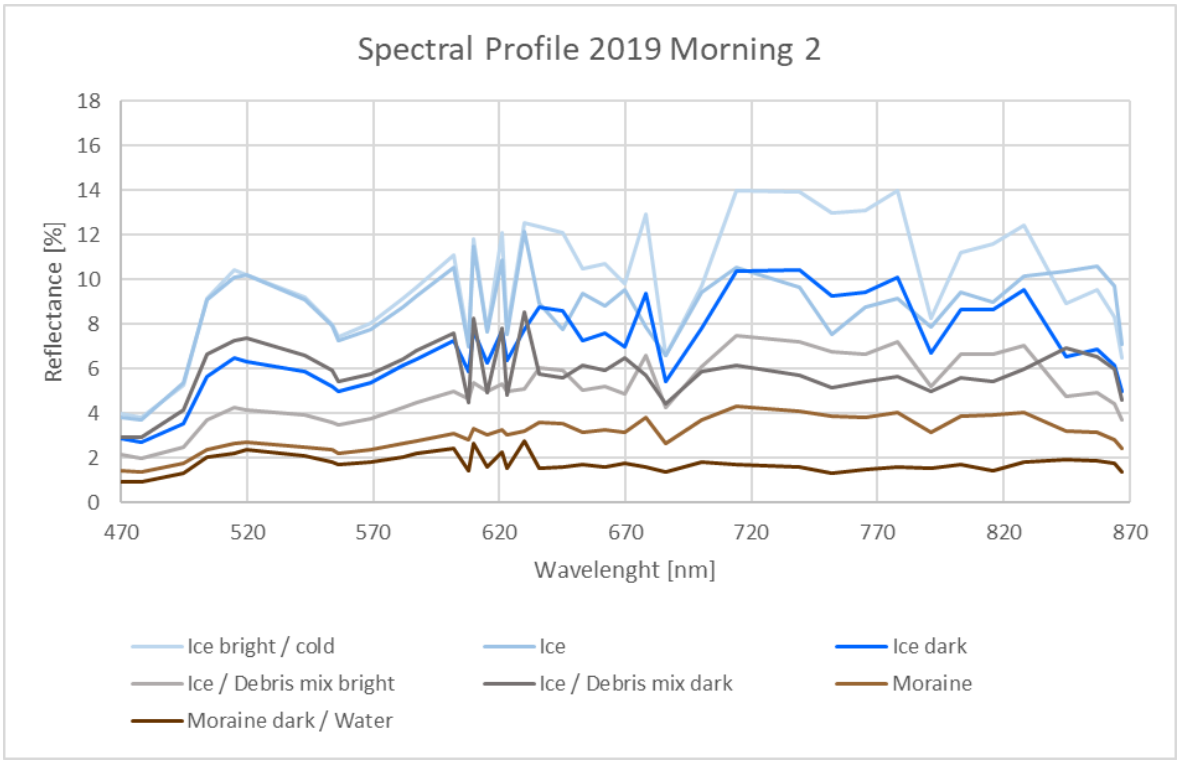

Figure 12: Spectral profiles based on the combined VIS and NIR classification for the second morning flight 2019.

The spectral profile of the second morning flight has two moraine classes, which have clearly lower reflectance values over the entire spectrum. The bright ice class has a similar profile like the it was found on the other 2019's flights. The same is true for the dark ice. The normal ice is following profile of the bright ice till 650 nm and changes then to the level of the dark ice. The profile of the bright mixture class has a similar shape than the two mixture classes identified in the first morning

flight. The dark mixture class shows first a spectrum like bare ice and then continues at a lower level than the bright mixture class.

2019 Morning Flight 3

Based on the spatial distribution of the surface classes, the classifier for the third morning flight worked the best out of the 2019 data. The classified images have detailed structures, where cracks and crevasses are and the deep channels are in a separated class.

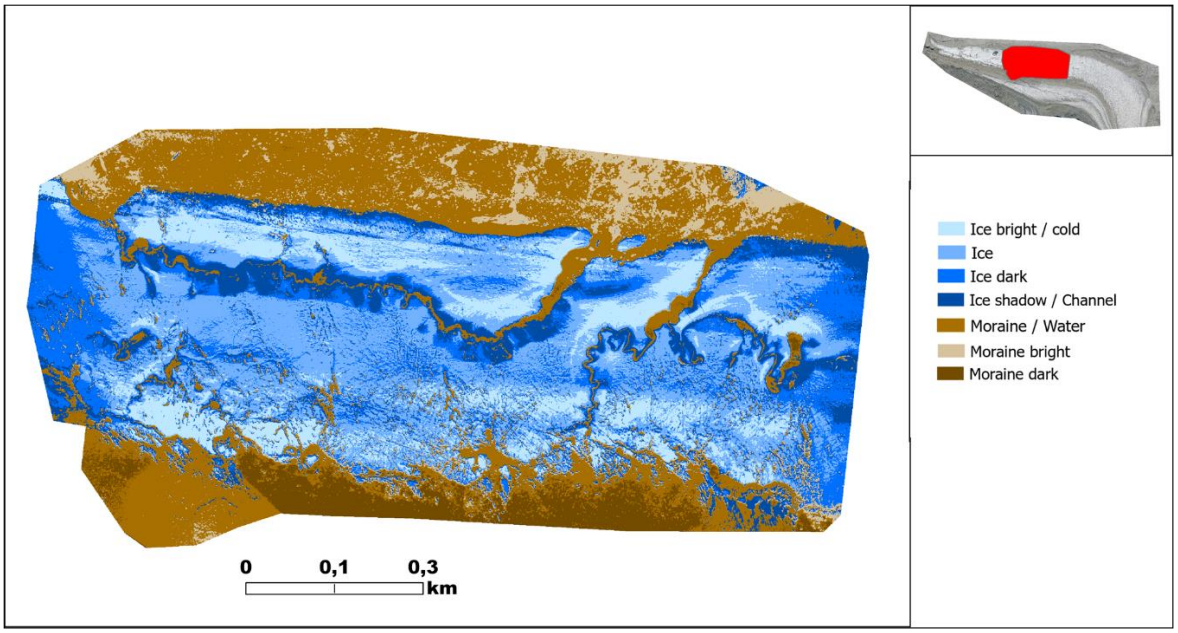

Figure 13: Classification for the third morning flight 2019 based on the combination of the VIS and NIR datasets.

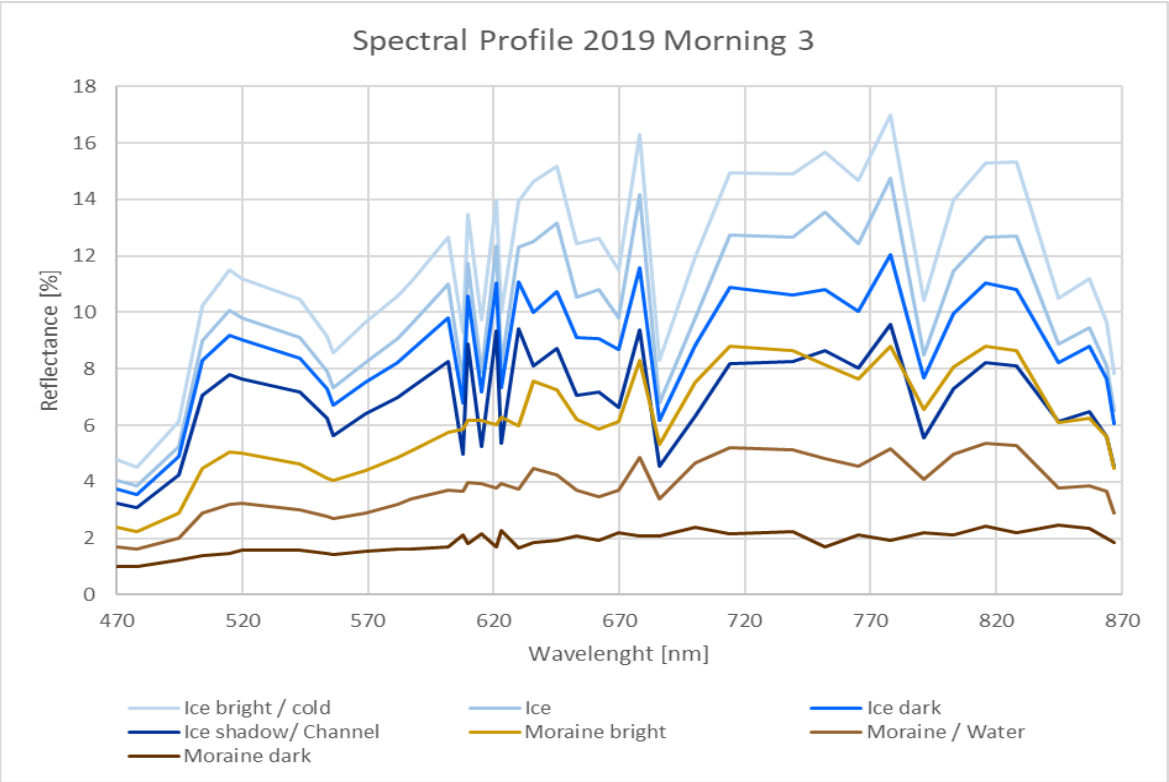

Figure 14: Spectral profiles based on the combined VIS and NIR classification for the third morning flight 2019.

The spectral profile shows clear separation of each surface class. The shapes of the four ice classes have similar shape, which are different from the shape of the moraine class at wavelength of 620 nm, 660 nm and 720 nm. The peaks and lows at 620 nm of the ice classes are missing for the moraine classes. At 660 nm ice classes are slightly peaking, while moraine classes have a slight drop in reflectance. At 720 nm moraine classes show a convex shape, while ice classes slightly concave.

2016 APEX

The image taken by APEX covers the whole lower ablation area of Grenzgletscher. The classification is carried out by including all 284 bands and has a spatial resolution of 2 m. Therefore this classification is based on finer and wider spectral resolution, but coarser spatial resolution, than the other classified images from 2019.

When looking at the RGB image (figure 15) of this flight, a slightly pink color on the tongue of Grenzgletscher is visible, this color occurs due to the band combination used to generate the RGB image and is not visible in the field. However this slightly pink area is a well representation of surface cold ice in the ablation of Grenzgletscher. The area covered by the APEX image contains also the tongue of Zwillingsgletscher, which lies next to the Grenzgletscher with a medial moraine in

between. The temperate ice of Zwillingsgletscher does not have any pinkish color, which supports the assumption, that the slightly pink color represents cold ice.

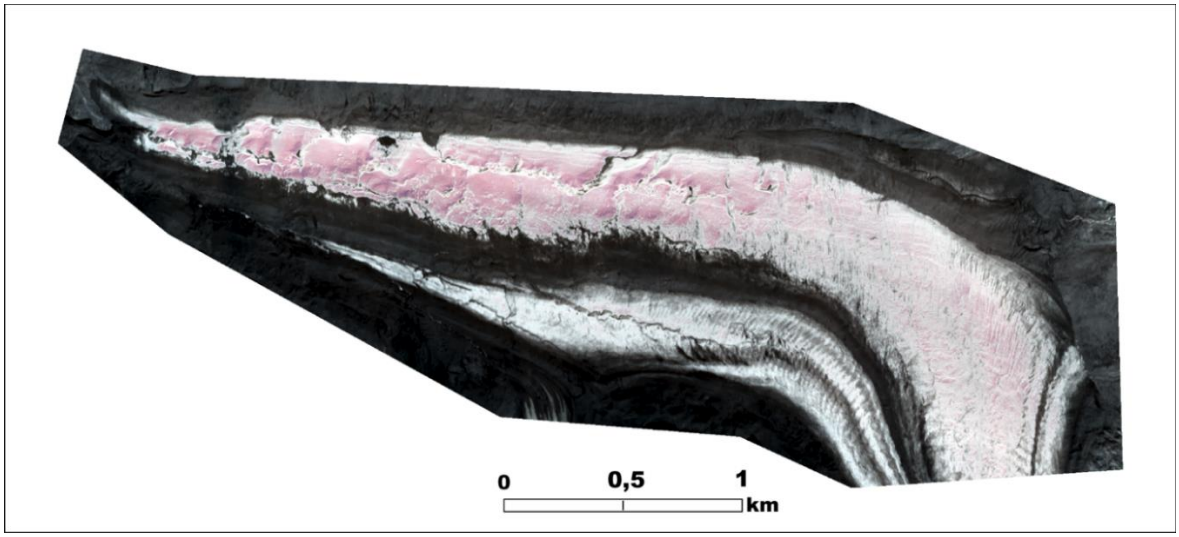

Figure 15: RGB image of the APEX dataset from 2016.

The classification of the APEX image resulted in 7 classes, representing 4 ice classes and 3 surrounding classes.

The 4 ice classes are also named after their brightness, while darker ice is mostly due to more dirty ice or shadow in crevasses or channels. The ice classes show a clear distribution. Bright / cold ice is mostly found in the glacier middle on the lower ablation area. Closer to the tongue bright ice seems to cover a larger amount surface area than higher up. In general the ablation area of Grenzgletscher is classified as followed, the classes decrease in brightness by a more lateral position on the glacier tongue. Ice structures like channels or crevasses are detectable, because they represent a darker class within brighter classes.

The 3 surrounding classes are named moraine bright, moraine and moraine dark, based on their brightness. They are called moraines, because the flights from 2019 covered mainly areas on the glacier and moraine. For the image the term moraine might be not the right, since the valley sides are also covered, but the material of the moraines and the mountain side are basically the same, because moraine material originates from this area.

It is remarkable that the classification did not classify a water class, because there is a lot of supraglacial water on Grenzgletscher. Water is known for low backscatter across the whole reflectance spectrum, which distinct water from ice or moraine material. In this classification water is mostly classified within dark moraine or moraine. This is maybe due to the spatial resolution of 2 m or the thin water layer.

The classifier of the APEX image seems to have problems with debris-covered glacier ice. This can be identified by comparing the RGB image and the classified image, regions for misclassifications

are at the sides of Grenzgletscher, the confluence area of Gorner- and Grenzgletscher, the tongue of Gronergletscher , the snout of Zwillingsgletscher and area covered by the medial moraines.

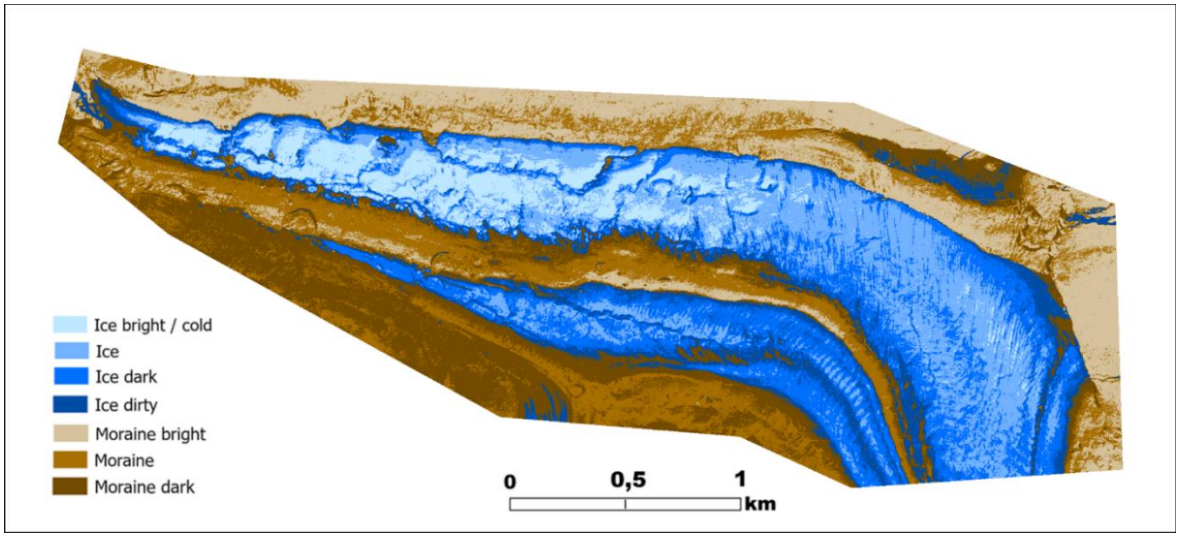

Figure 16: Classification of the APEX dataset form 2016.

5.1.2 Comparison of Classification results for different cameras

The comparison of the classification results is made for the VIS, NIR and combination for each flight separately. It needs to be mentioned that the values of combination dataset was calculated from the VIS and NIR dataset, which have a different spatial resolution. The values were generated by creating a dataset which contains the 16 bands from the VIS, and 25 from the NIR dataset. The spatial resolution is the same as the NIR image, and the values for the VIS bands have been chosen with the nearest-neighbor method. However there is a spatial bias between the VIS and NIR dataset, which is recognizable in an offset glacier surface features. This offset is varying in size and direction und can be up to a few meters in ground distance. The removal of the offset by different attempts of re-geolocation based on surface features failed and also the manual attempt by creating fitting points could not solve it. Therefore this offset is recognizable in the classifications of the combination images.

5.1.2.1 VIS, NIR and Combination classifications 2019

2019 Evening Flight

The most obvious difference between the classification of the VIS, NIR and combination datasets is, that the VIS classification shows much more detailed classes, while the NIR classification seems more smooth. The VIS classification shows class distinction in between the ice classes, based on shadow and topographic effects. An example for this, is the depression between the great supraglacial

lake and the center of the tongue. But the VIS classification provides good results in identifying bare ice. The NIR classifier on the other side, seems to have problems in the differentiation of dirty ice from debris. According to the NIR classification, the supraglacial lake is placed half on ice and half on moraine material. The shading effects found in the VIS classification do not appear in the NIR classification. The combined classifier is a mixture of both, it shows finer surface structures than the NIR classifier but keeps the smoothening and does not reproduce the shading effect of the VIS. Due to the offset of the integrated datasets, rocks are sometimes not assigned to a moraine class. This is mainly due to the size of the rock and the offset, so that the rock from VIS is placed next to the rock form NIR.

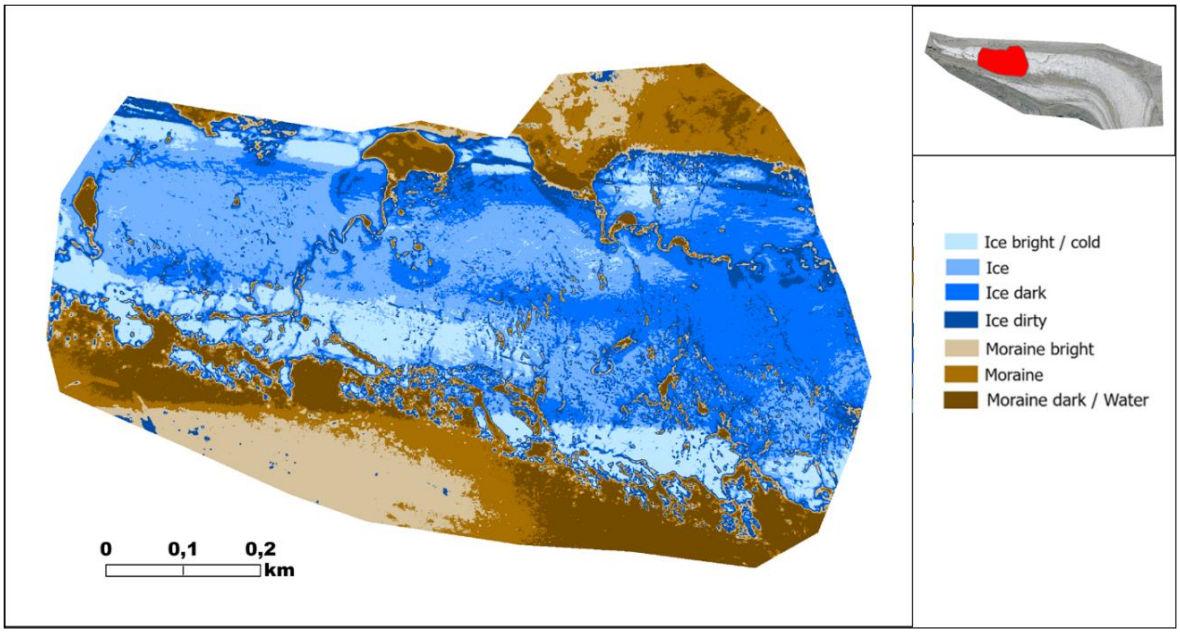

Figure 17: Classification for the evening flight 2019 based on the VIS dataset.

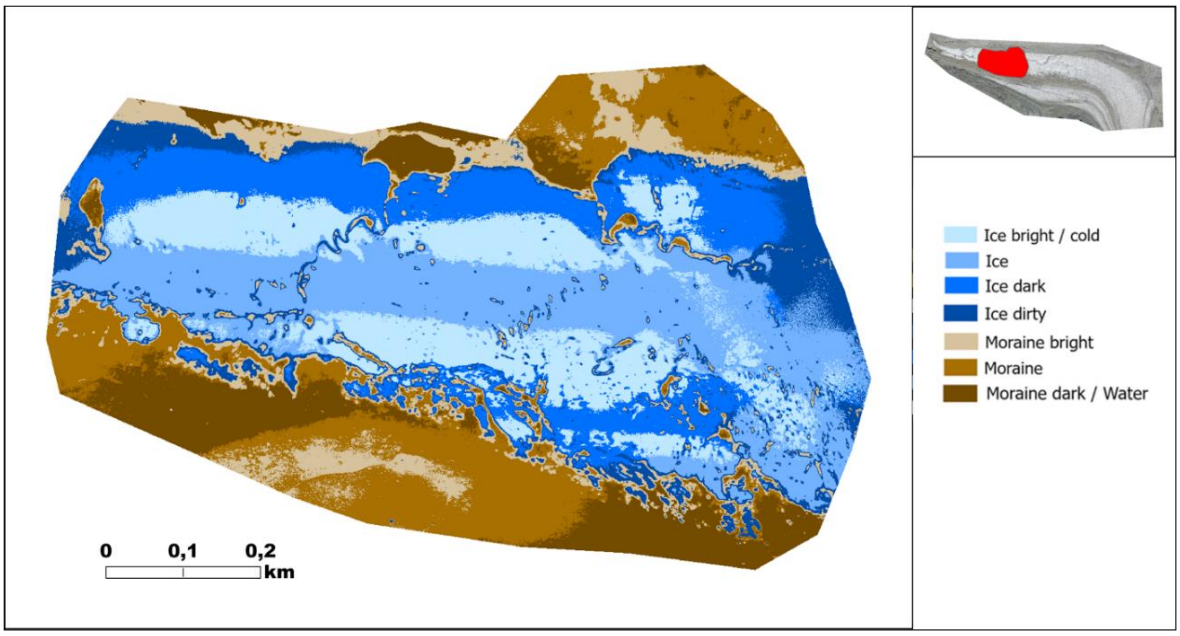

Figure 18: Classification for the evening flight 2019 based on the NIR dataset.

2019 Morning Flight 1

While the VIS and the combination classifications contain mixture classes, the NIR classifier did not produce those classes. The NIR classes appear more uniform and consistency, than the VIS and combination classification, which is highly variating on the glacier surface.

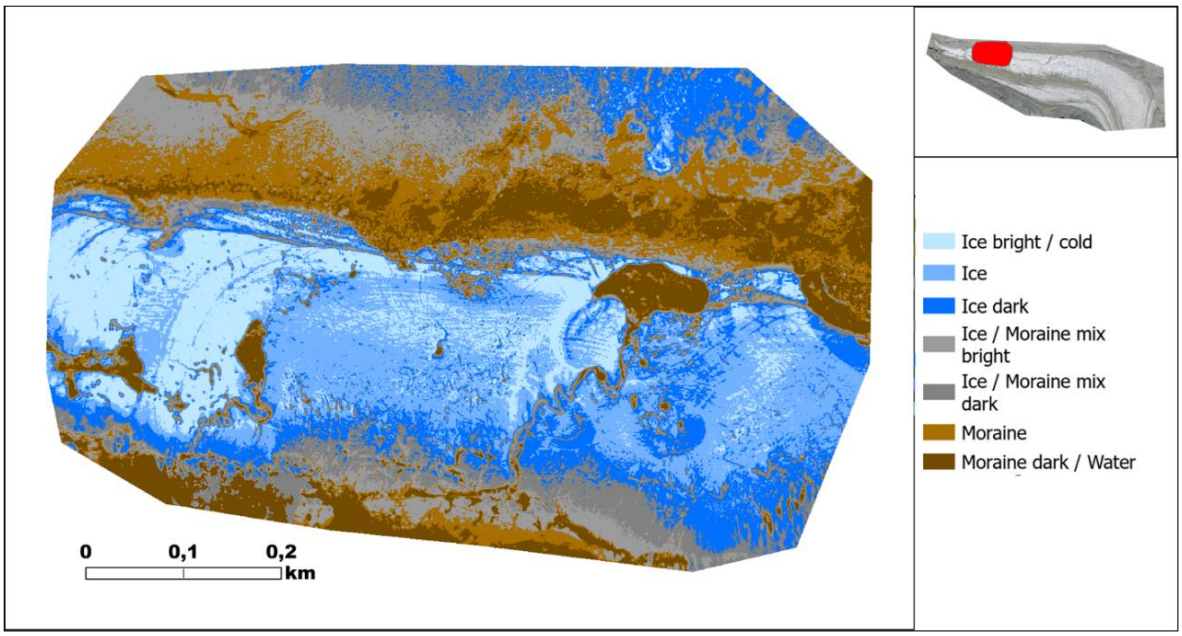

Figure 19: Classification for the first morning flight 2019 based on the VIS dataset.

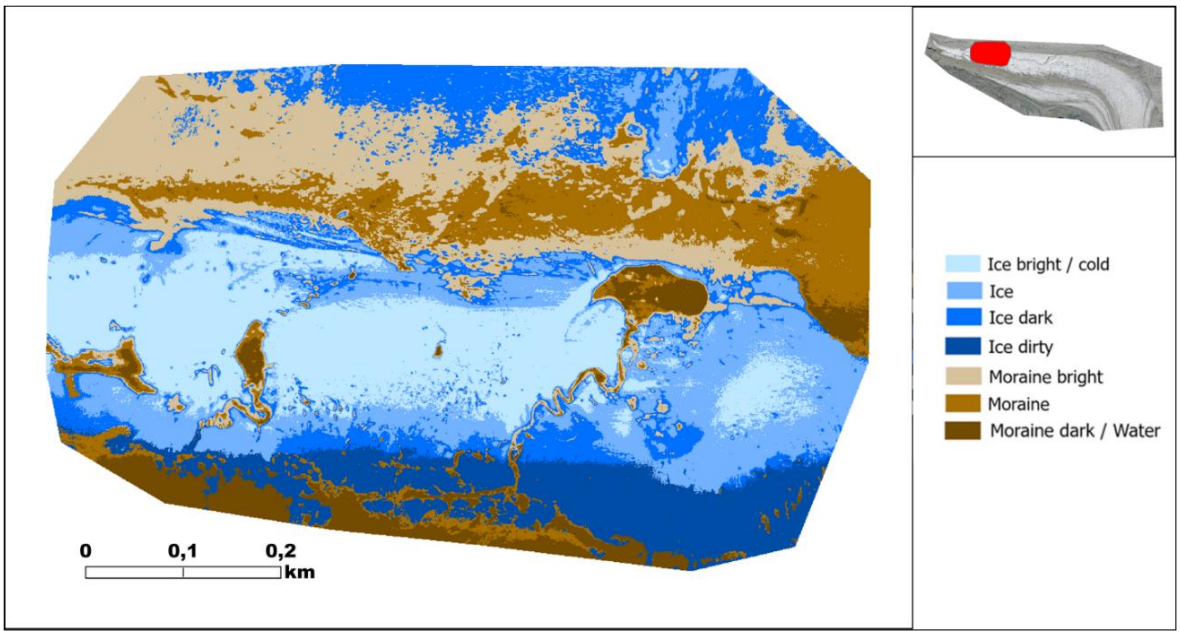

Figure 20: Classification for the first morning flight 2019 based on the NIR dataset.

2019 Morning Flight 2

The three classifiers produces similar patterns in general. The VIS image shows the smallest amount of bright ice and much more dark ice in the center of Grenzgletscher. The two moraine classes have almost the same extent on the three images. While the VIS image mapped mixed material in the shadowed area on the valley side of Grenzgletscher, the NIR classifier detected much more mixed surface on the center part of the glacier.

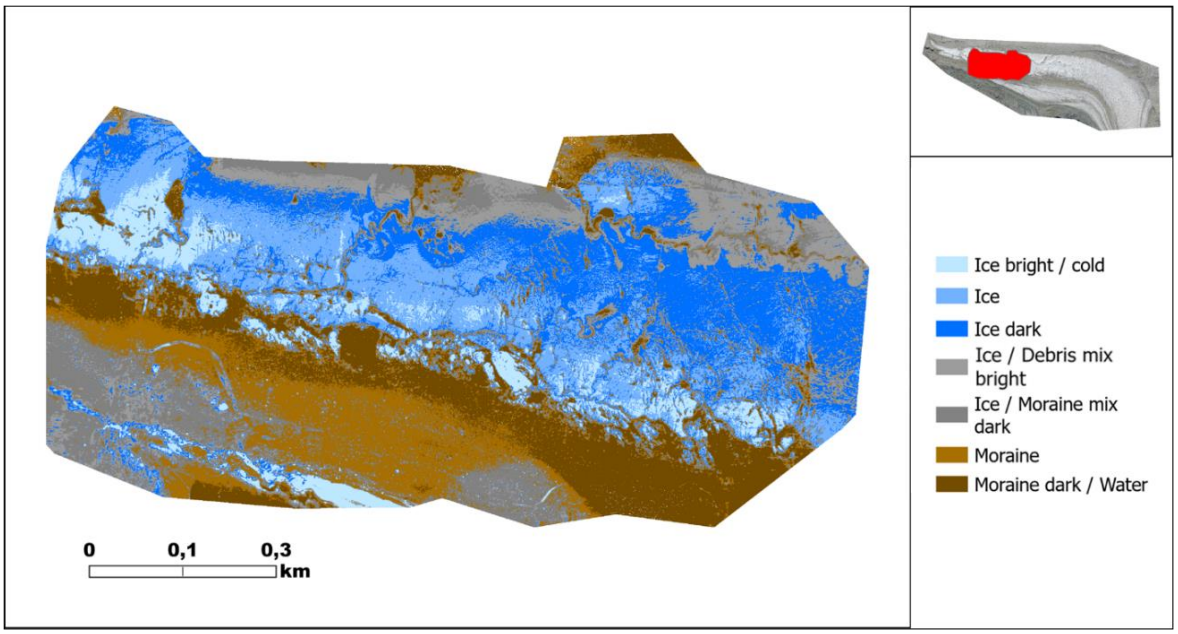

Figure 21: Classification for the second morning flight 2019 based on the VIS dataset.

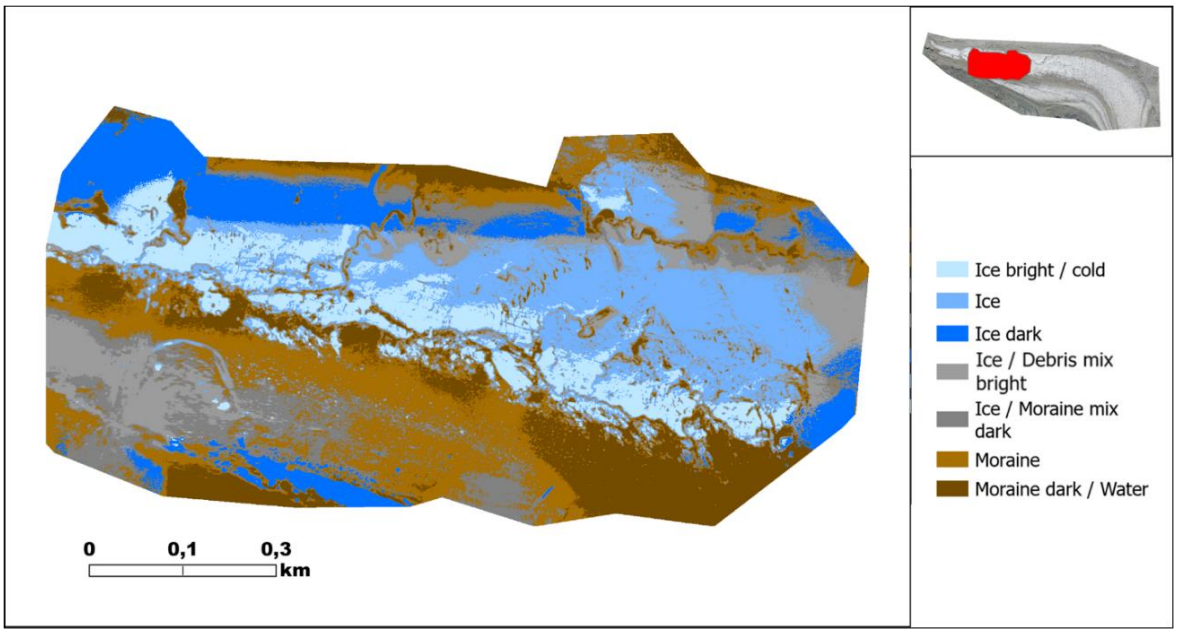

Figure 22: Classification for the second morning flight 2019 based on the NIR dataset.

2019 Morning Flight 3

The classifications of the third morning flight 4 ice classes and 3 moraine classes. For the VIS classification there is instead of a third moraine class an ice debris mixture class. The moraine classes of all three classifiers are covering almost the same area, varying only by the assignment within the moraine classes. All three classification images assigned darker classes to crevasses and cryoconite holes, than to the surrounding area. The darker band of impurified ice at the glacier margin is clearly recognizable in all classifications.

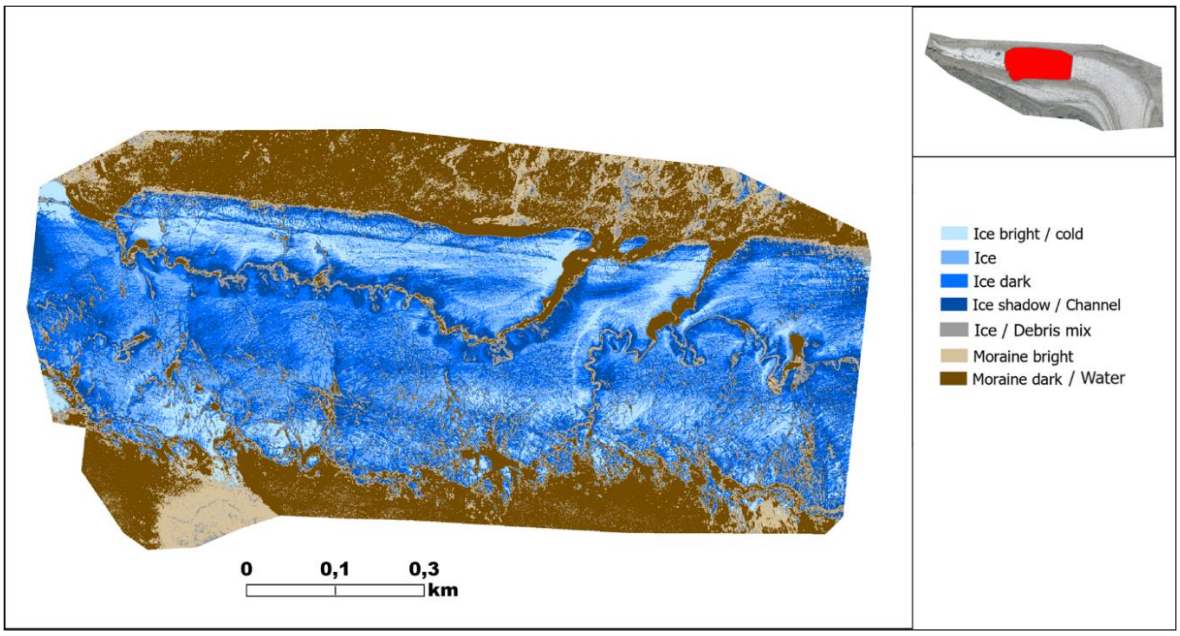

Figure 23: Classification for the third morning flight 2019 based on the VIS dataset.

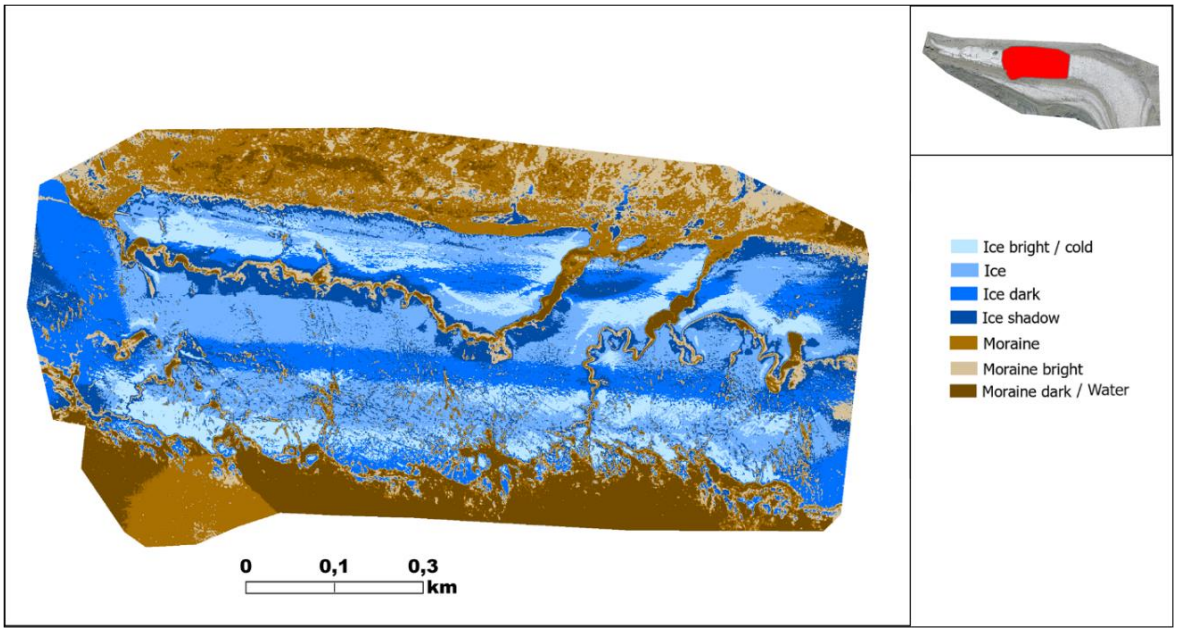

Figure 24: Classification for the third morning flight 2019 based on the NIR dataset.

5.1.2.2 Differences campaign 2016 and 2019

The classification of the APEX dataset form 2016 is based on 284 bands and a ground resolution of 2 m, while the 2019 datasets contain 16 VIS and 25 NIR bands with a ground resolution of 0.6 to 0.75m. The classification for the APEX dataset was performed over the whole study area, this means that the training of the classifier used all information about the entire ablation zone. While the classification for the 2019 datasets was based on smaller areas, which may produce more classes for

the study area, than that area would contain based on the APEX classification. Based on the coarser ground resolution the APEX classifier only identifies the largest rocks, with diameter > 2 m and summarized surface structures with smaller scale. The APEX classification performs well in identifying bare ice and outperforms the other classifier in dirty ice and slightly debris-covered areas.

5.2 Thermal Images

The thermal images were not further processed and directly used. The interpretation of the thermal images is based on comparing the thermal signals to the corresponding RGB image. This was sometimes difficult, because the light conditions on the RGB images from 2019 were not perfect, therefore additionally aerial images were consulted. The temperature measured of the drone flights seem to be od and the temperature is therefore interpretated with relative terms like warmer and colder.

5.2.1 General overview (Surface Structures and temperature)

2018

The thermal image from 2018 shows similar thermal distribution as Ryser et al., (2013) describing. The ice in the center of the glacier is coldest and gets warmer towards the margins and the medial moraine. Also the warming of the ice along the flow line downwards is mapped. The thermal image is ideal to identify debris on the glacier, also singe rocks, because they absorb more solar energy and heat up during the day. This makes rock recognizable as warm spots on cold glacier ice. On an closer look there are there are slightly warmer areas, within the glacier. This areas can be assigned to cryoconite, sediments and water bodies. All those materials have a lower albedo than glacier ice and therefore absorb more solar energy. The temperature values measured are clearly wrong and do not represent surface ice temperature, since they are positive all over the glacier. A closer look to areas of interest will be taken in chapter 5.3.

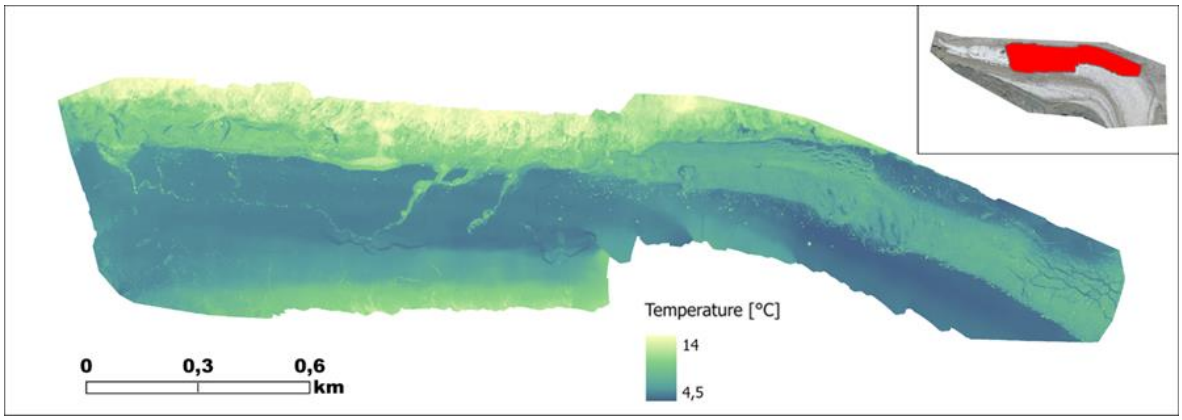

Figure 25: Thermal image acquired during afield campaign in 2018.

Figure 26: RGB image of acquired during a field campaign in 2018.

2019 Evening Flight

The thermal image of the evening flight 2019 shows a strong thermal gradient from the coldest center part of the glacier to the warmer margins. The much warmer spots represent rocks and debris, which has warmed up during daytime. There are also colder areas within the ice, when comparing their position to the RGB, this areas represent cryoconite holes. The general temperature distribution is reliable for this area.

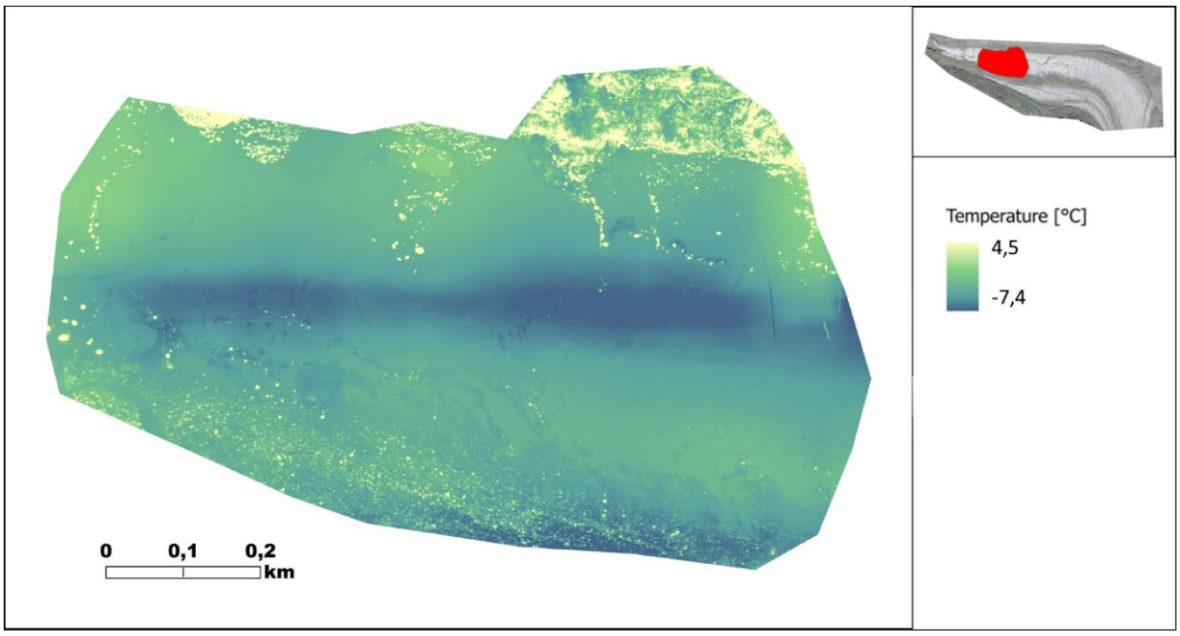

Figure 27: Thermal image of the evening flight 2019.

Figure 28: RGB image of the evening flight 2019.

2019 morning flight 1

The thermal image form the first morning flight is located at the margin of the glacier ice. The moraine material is clearly warmer than the glacier or material on the glacier. The temperature difference between rocks on the glacier and the glacier ice seems to be smaller than in the evening image. This indicates a cooling of the rock and debris over the night. The thermal image also mapped that supraglacial lakes have lower temperatures than the surrounding glacier ice. This can be due to

the accumulation of cold air in a depression. The lower right half of the image seems to be biased, due to errors introduce in the processing of the data.

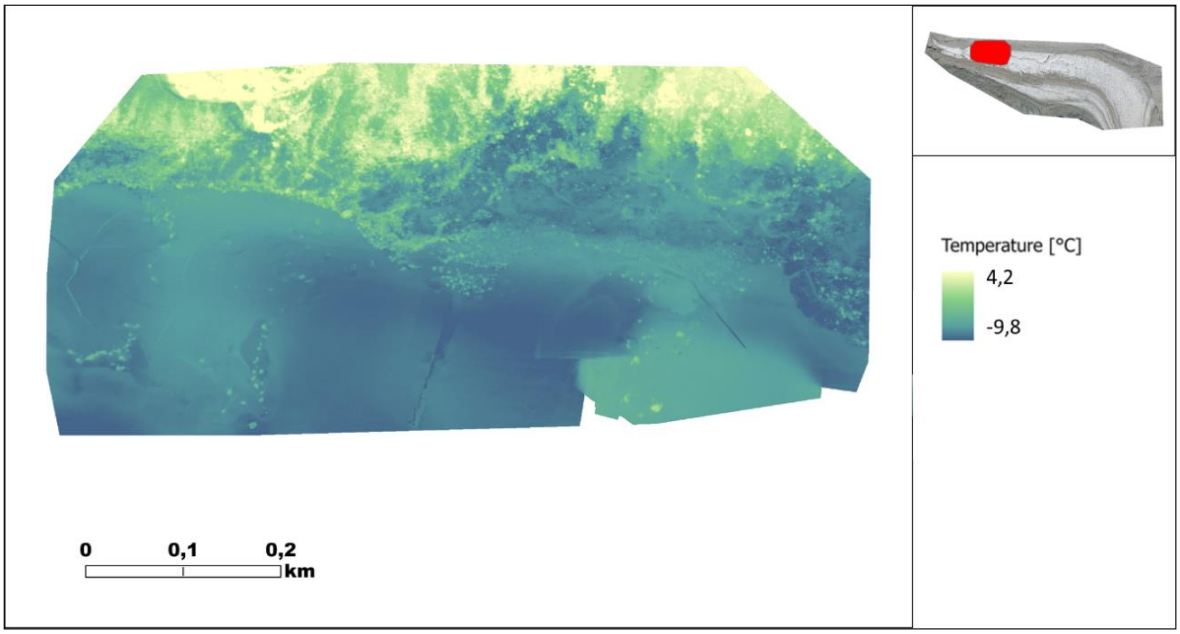

Figure 29: Thermal image from first morning flight 2019.

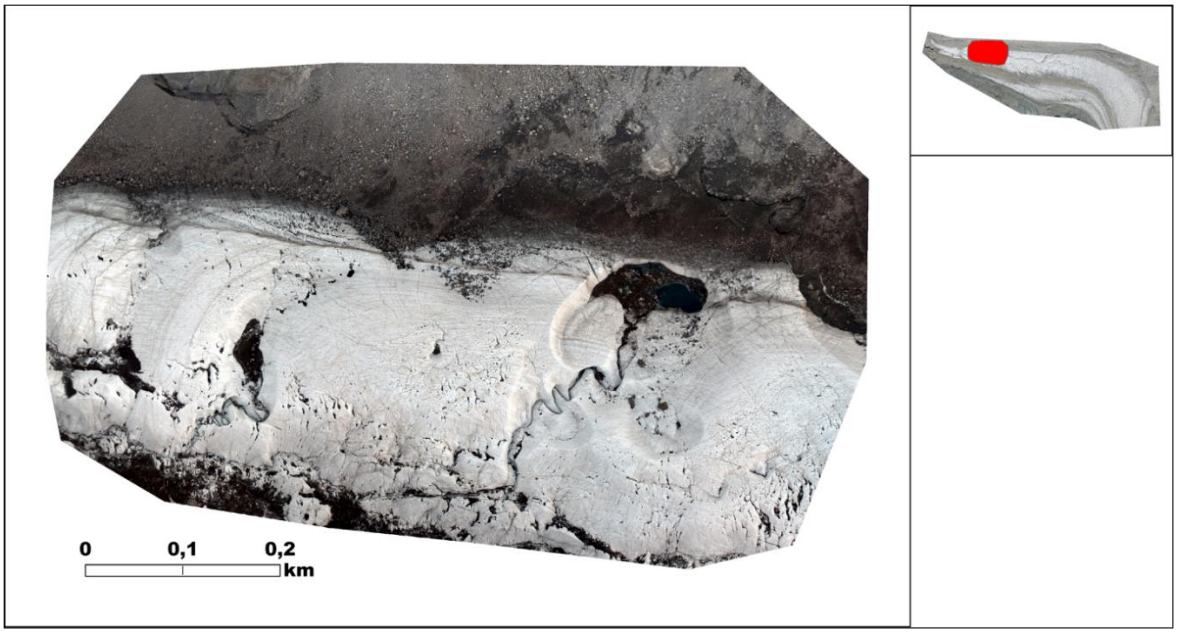

Figure 30: RGB image from first morning flight 2019.

2019 morning flight 2

The second morning flight mapped the colder temperature at the center of the tongue with increasing temperatures towards the margins. The cold temperatures over the moraine and close to the valley wall seem to be biased. There are also rocks towards the snout, which are mapped twice on the

thermal image. The temperature patterns is similar to turbulent water and compared to the other thermal images much more vague.

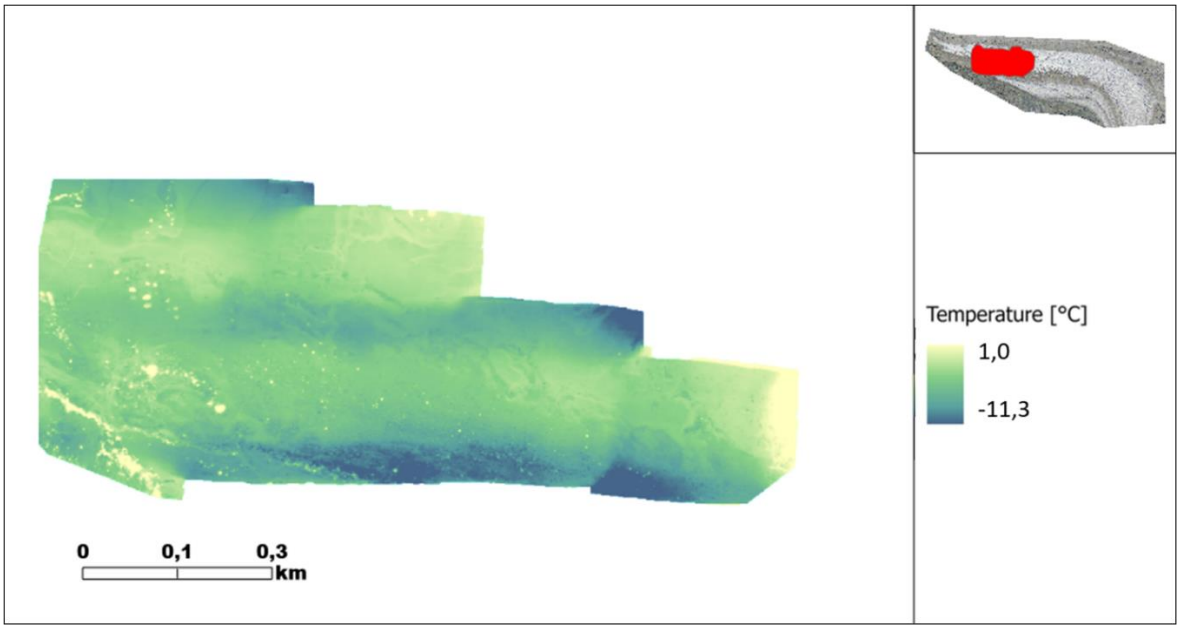

Figure 31: Thermal image from second morning flight 2019.

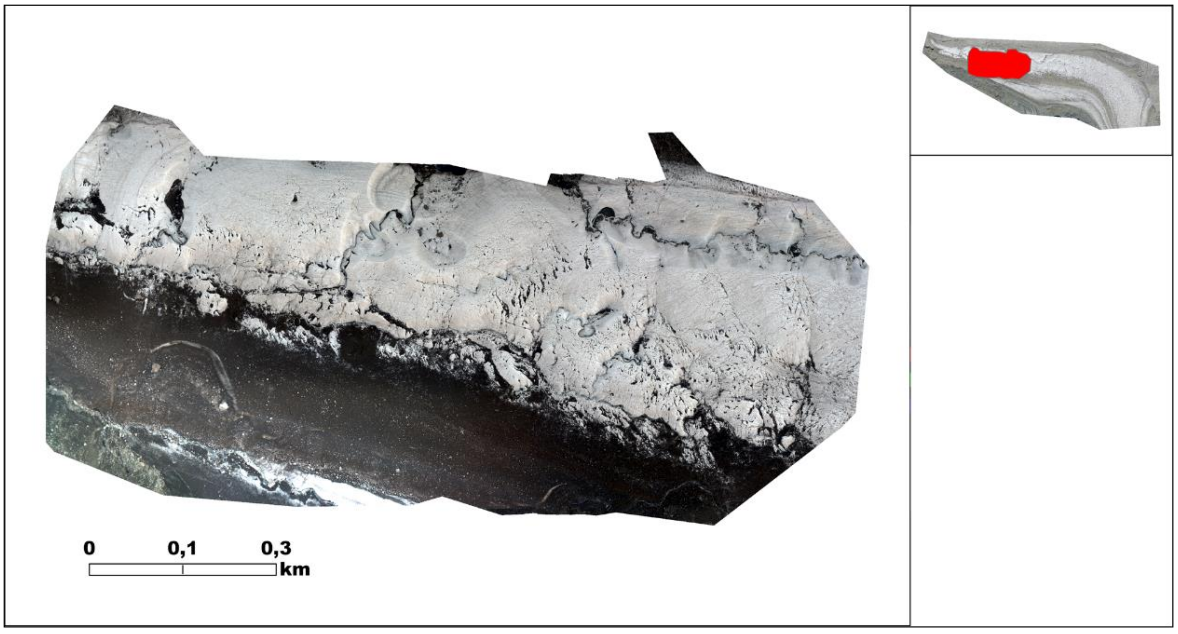

Figure 32: RGB image from second morning flight 2019.

2019 morning flight 3

The third morning thermal image is from the area of the large meltwater channel. The areas where sediments are accumulated are colder than the surrounding ice. There also rocks, which have fallen

from the valley sides, on the glacier, surprisingly not all of them have a warmer spectral signature, some even show colder temperature thant the surrounding ice.

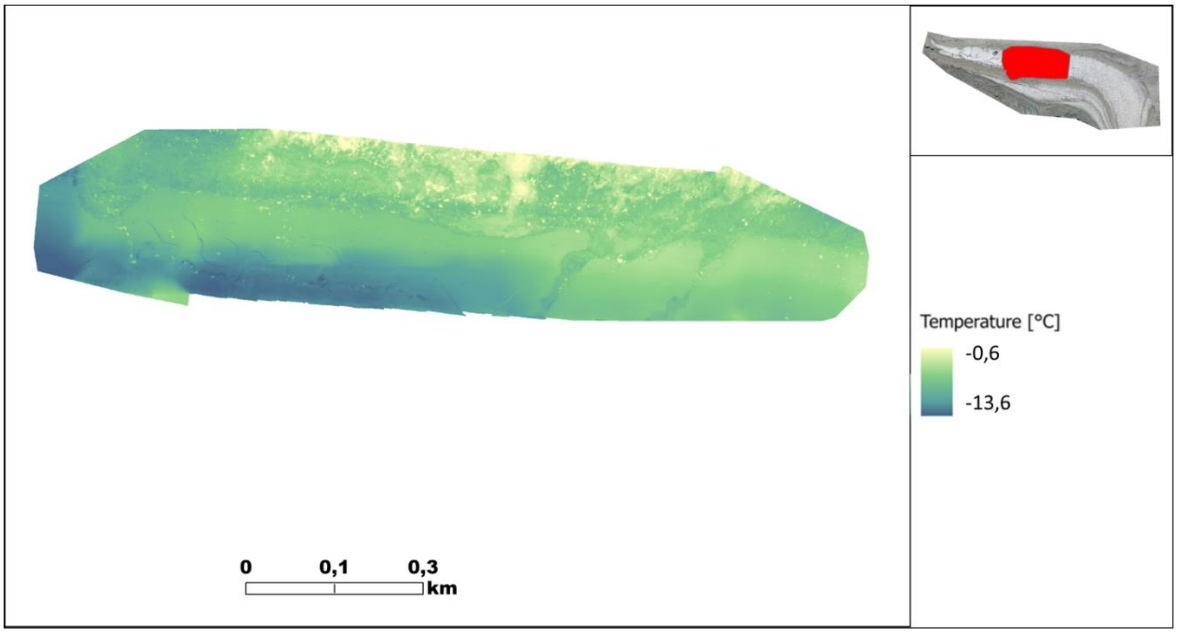

Figure 33: Thermal image from third morning flight 2019.

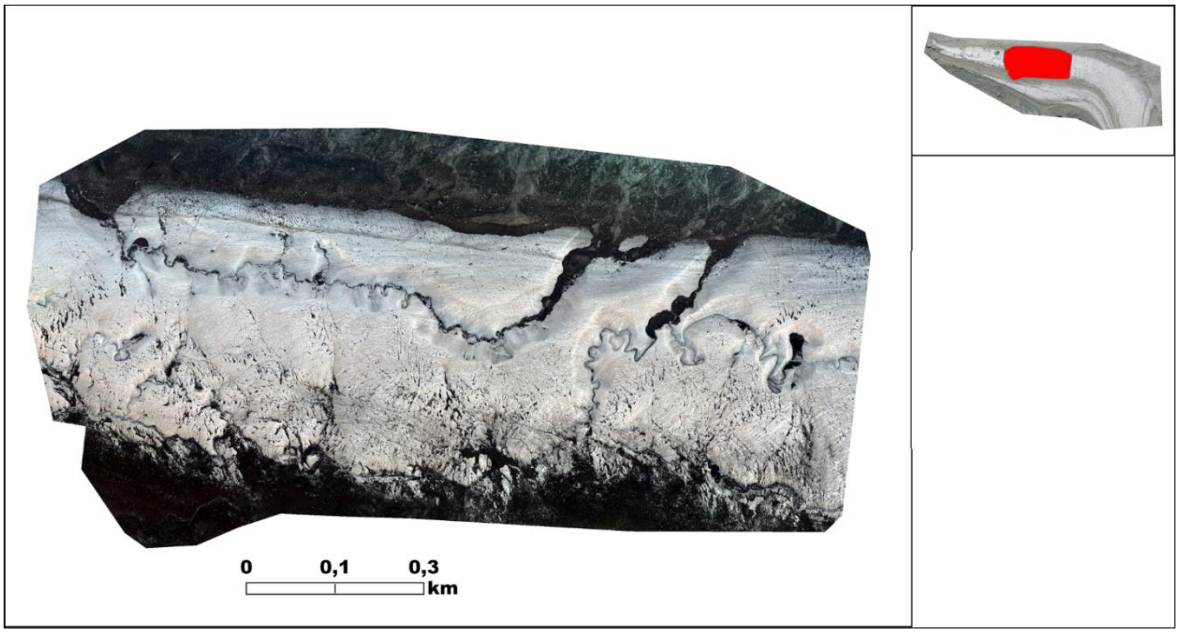

Figure 34: RGB image from third morning flight 2019.

5.2.2 Thermal Ghosts

In several thermal images structures can be found, which cannot be connected to any surface structure or elevation features. This features only occur on glacier ice and appear as long linear features which are 1 – 2 °C colder then the surrounding area. They can be found in all thermal images used in this

thesis and also occur on similar regions. When investigating these features by looking for them in the single original images taken by the drones, the are not present. According to that fact, they are interpreted as errors caused by the mosaicking of the thermal images.

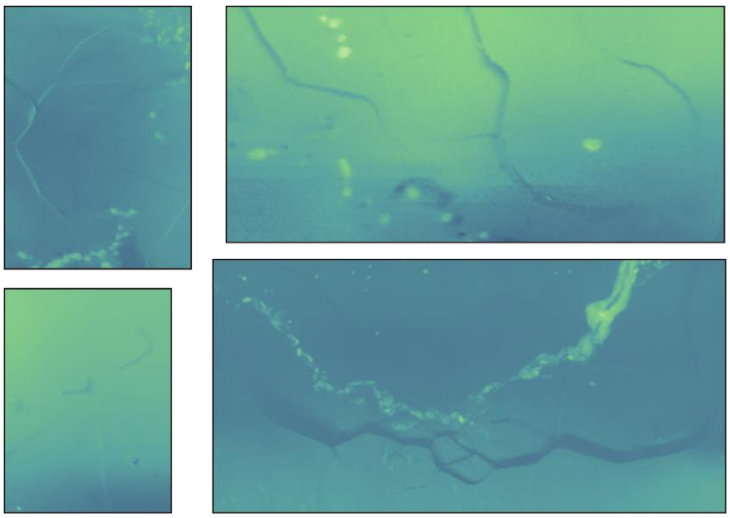

Figure 35: Thermal ghosts, error features causes by the mosaicking of the thermal pictures.

5.3 Surface Structures

Surface structures and their position on the glacier are explored by using five areas of interest, which are characterized by either interesting surface or thermal structures or challenges in classification.

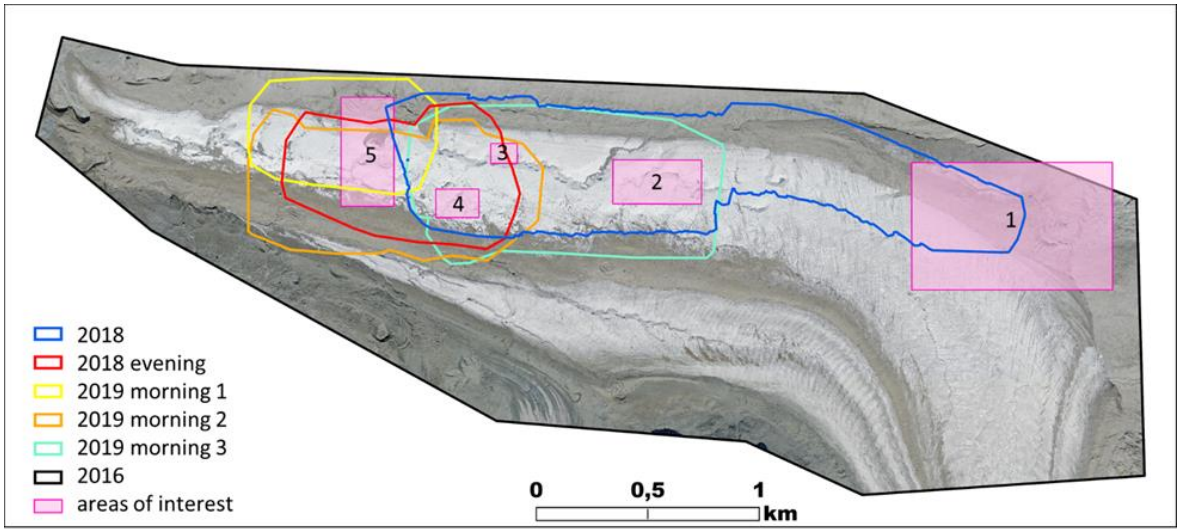

Figure 36: Overview of the study area, the outlines of area covered by the drone flight and the study site of the areas of interests are located on the lower ablation zone of Grenzgletscher.

Study site 1

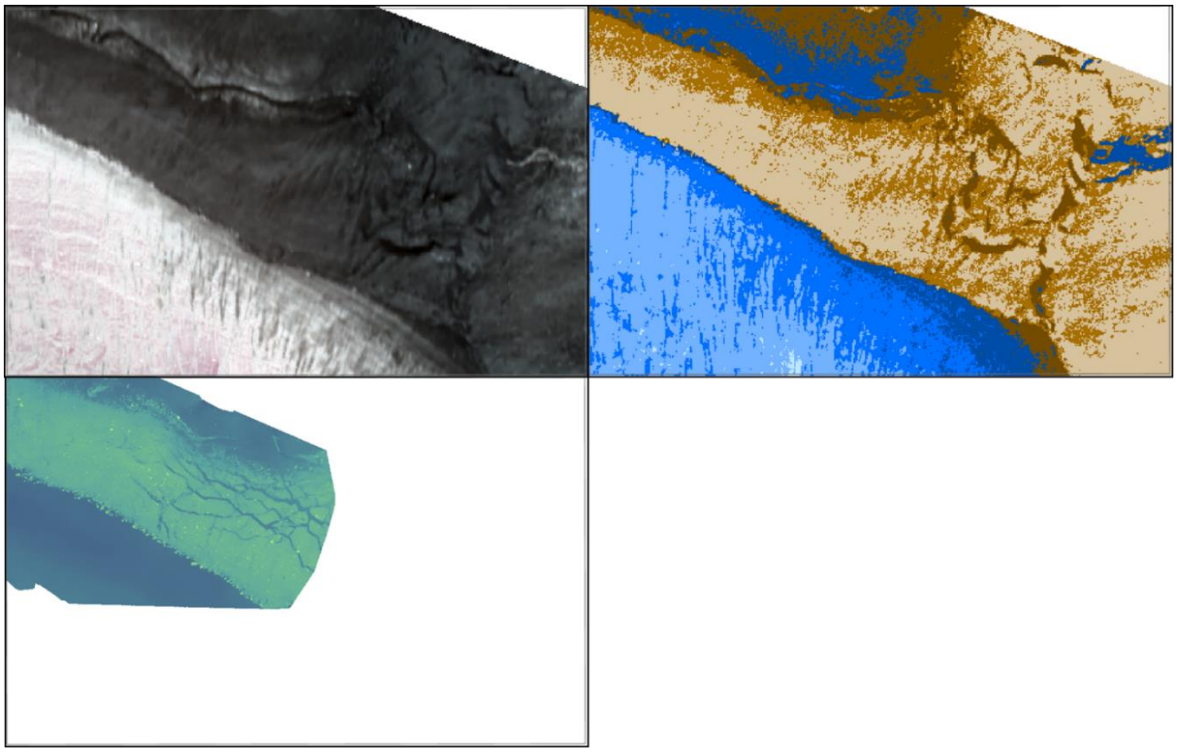

Figure 37: Study site 1, APEX RGB (top left, fig. 15), classification APEX (top right, fig.16) and thermal image from 2018 (bottom, fig. 25). The legends to the single images can be found at the original figure.

This site was chosen, because of the dominant features in the thermal image from 2018. This thermal image is compared to the APEX image from 2016 and the classification results of it. The glacier ice is a homogenous cold feature in the thermal image, close to the moraine some rocks, which have fallen onto the ice, can be clearly identified because of the higher temperature. Within the moraine material cold cracks are visible. In the RGB image or the classified image, these cracks seem to be darker material or holes within the moraine. The thermal image shows similar temperature for glacier ice as for the cracks, therefore the thermal image indicates ice, while the classification tends to darker moraine. The pictures (see Figure 35) show that these cold cracks in the thermal image are indeed glacier ice.

Figure 38: Ice covered by the medial moraine at the former confluence zone of Gorner- and Grenzgletscher.

Study site 2

At this site the characteristics of deep meltwater channels are analyzed. While the classification with the APEX dataset fails to identify other material than ice, the multispectral classification groups all the non ice surface as moraine. There is no water detected (see Figure 40), even when this feature the out come of melt water fluxes. It is interesting, that the multispectral classification identified different material in the meltwater channel. The dark sports above the right pond are interesting, since their identification is difficult. The thermal image of 2018, shows one hot feature among several warmer features. While the hot feature is clearly a rock, the other are more likely cryoconite holes.

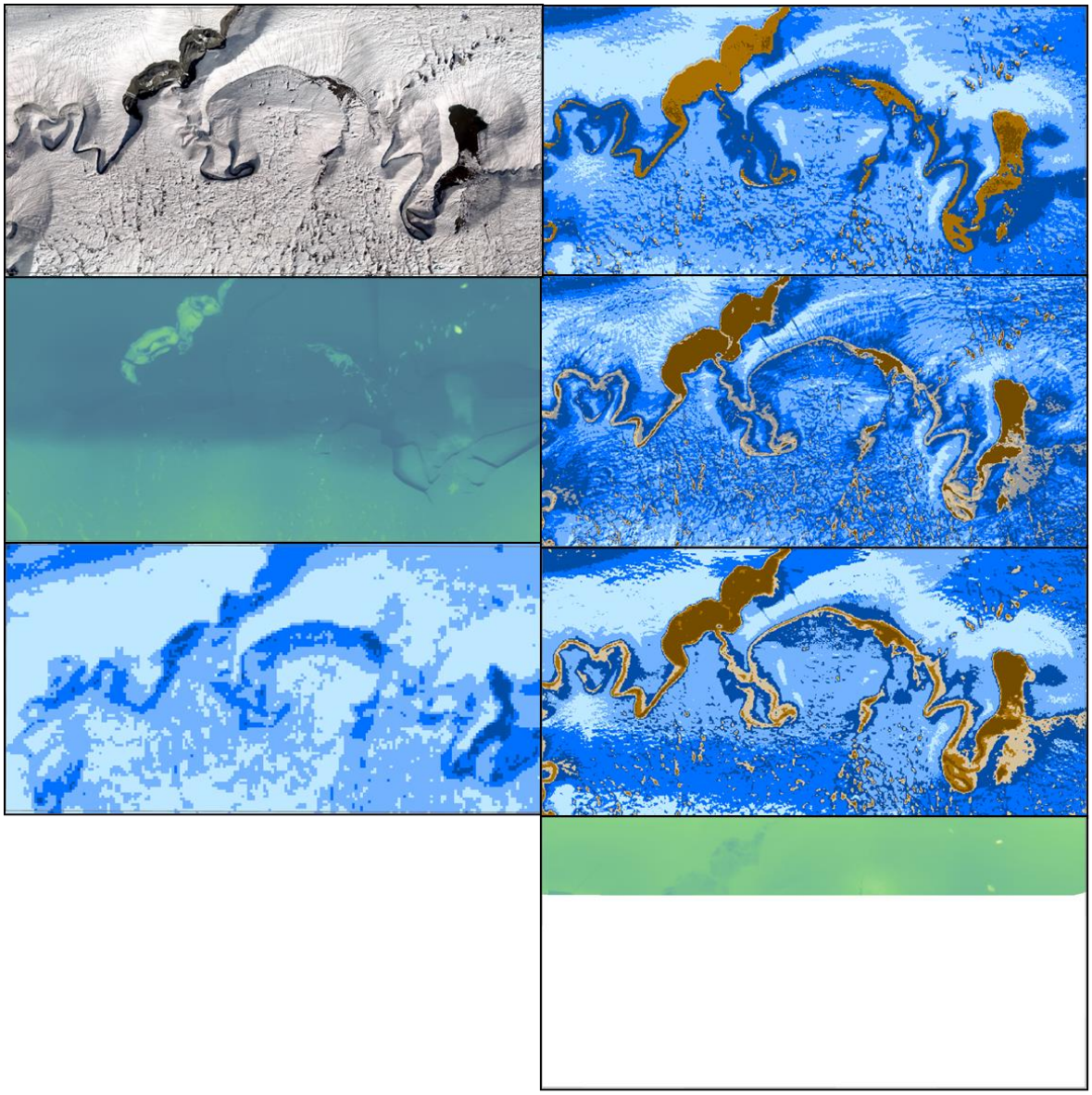

Figure 39: Study site 2, left side downwards: RGB image 2018 (fig. 26), thermal image 2018 (fig. 25), APEX classification (fig. 16); right side downwards: Morning flight 3 classification combination, VIS, NIR and thermal (figures 13,23,24,33). The legends to the single images can be found at the original figure.

Figure 40: Supraglacial pond within a channel system on Grenzgletscher.

Study site 3

This study site is covered by an evening flight and one morning fight and an additional thermal dataset form 2018 is given. The thermal pictures clearly show the diurnal temperature change of the debris. In the evening image, debris is much warmer than the surroundings, while in the morning this difference is smaller, the 2018 thermal image represents a situation on midday. Also the accumulation of cold air in depressions can be seen in the thermal pictures. There are also significant classification difference between the evening and morning datasets. The evening classification is much more homogenous than the morning classification.

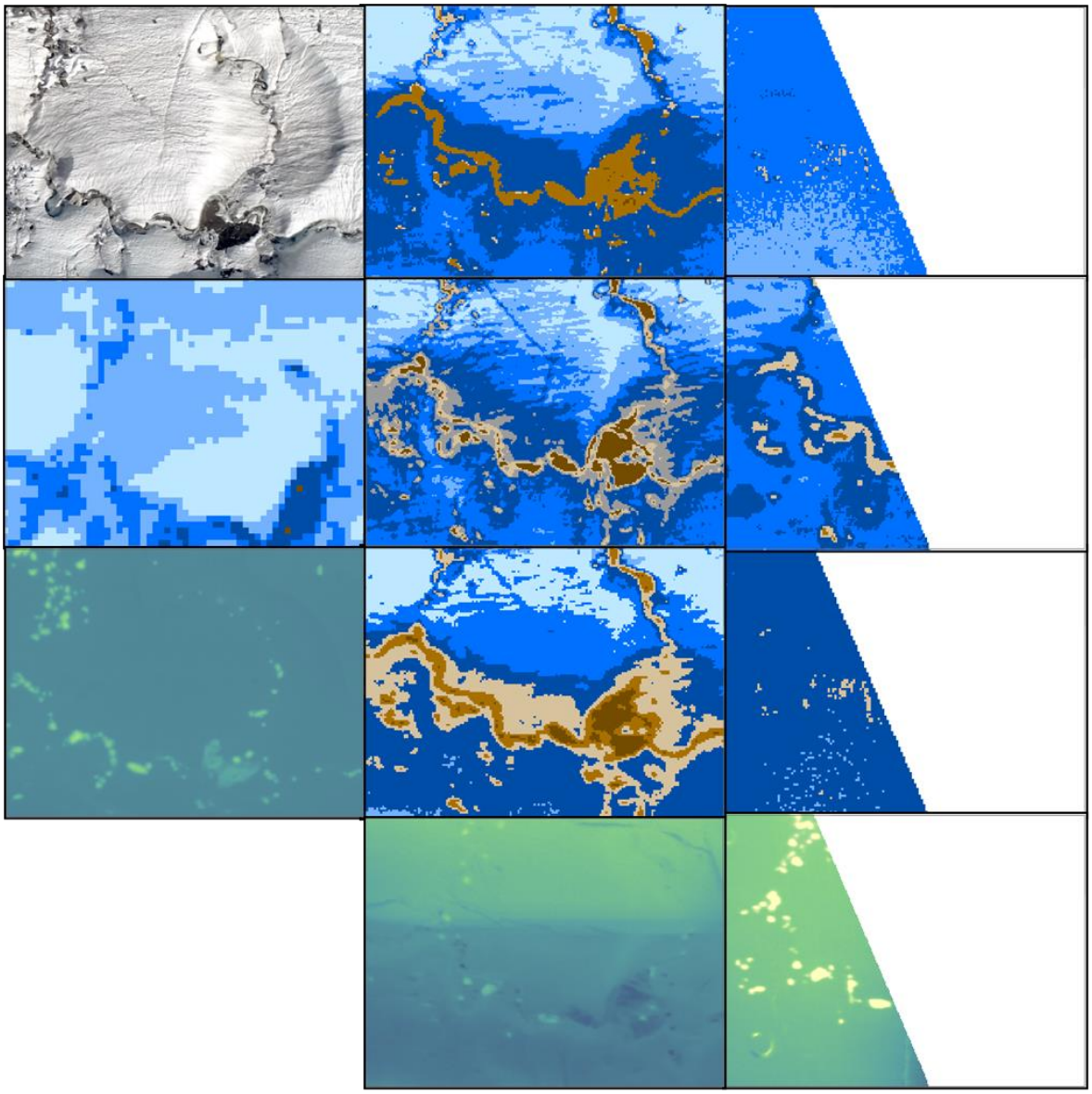

Figure 41: Study site 3, left side: RGB 2018 (fig.26), APEX classified (fig.16), thermal 2018 (fig 25); middle: Flight 3 combination, VIS, NIR, thermal (figures. 13, 23,24,33); right side: evening flight combination, VIS, NIR, thermal (figures 7,17,18, 29). The legends to the single images can be found at the original figure.

Study site 4

This site is located in an area rich of cryoconite holes. There is also a difference between the temperature of the cryoconite on the evening image compared to the midday image. The classification of the 2019 images seems to be influenced by shading effects, since the lower part is mostly classified as bright ice, while the APEX classifies almost the whole area in this category. The detailed classifications from the 2019 images illustrate that a finer classification not necessarily help and that this kind or results is far to fine for some application concerning a large area.

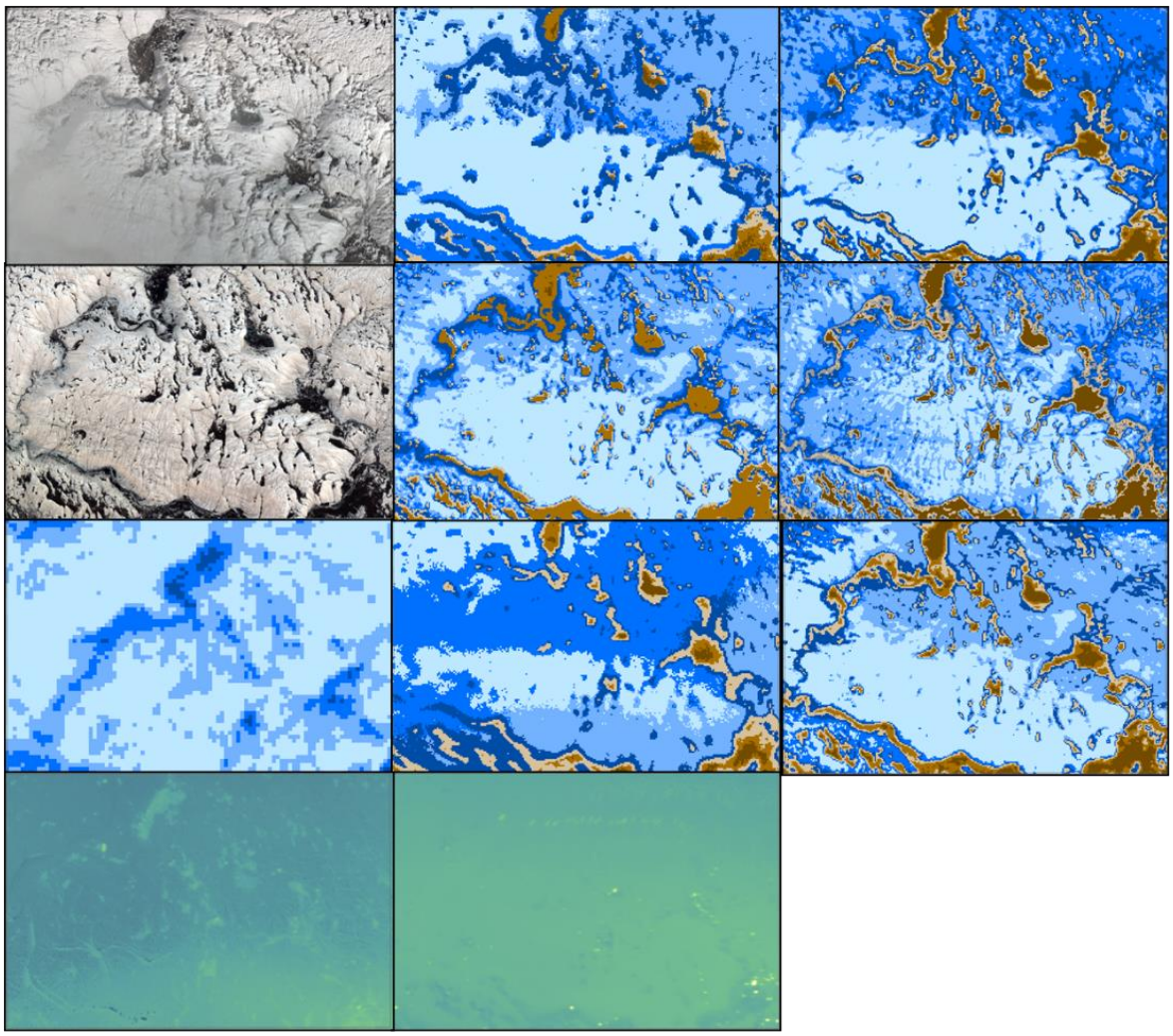

Figure 42: Study site 4, left side: RGB 2018 (fig.26), Fligth 3 RGB, (fig.34), APEX classified (fig.16), thermal 2018 (fig 25); middle: evening flight combination, VIS, NIR, thermal (figures 7,17,18, 29); right side: Flight 3 combination, VIS, NIR, thermal (figures. 13, 23,24,33). The legends to the single images can be found at the original figure.

Study site 5

This study site is supposed to give a closer impression about the north-south influence on deep meltwater channels. The hydromorphic feature starts at the higher center of the glacier and continues downward to the side of the glacier. According to the thermal pictures and Ryser et al. (2013) the glacier ice is getting warmer towards the lateral margin. Due to this flow direction, impurities are

getting transported to the glacier side, which confirms the darker ice classes on the glacier margins. In general, glacier surface structures shaped by meltwater tend to get bigger with more lateral position on the glacier. This is also due to the fact, that downstream more meltwater has been acquired then further up the system.

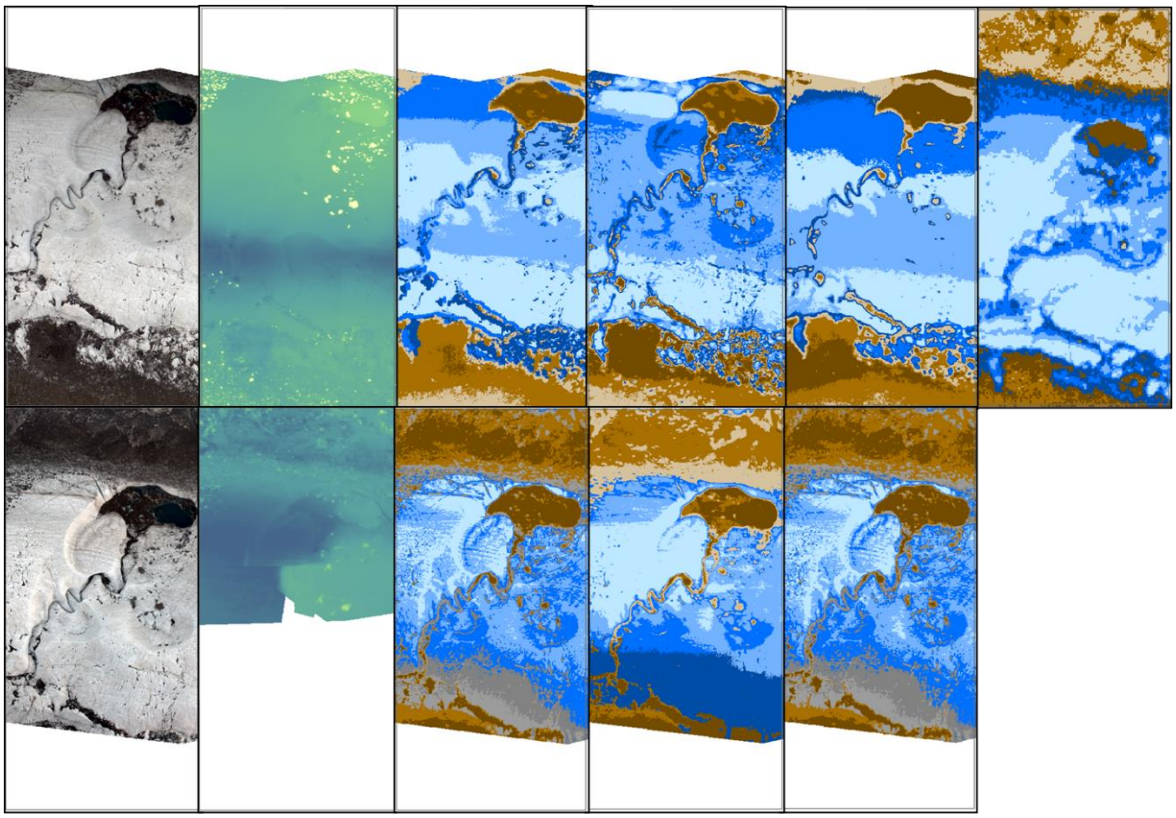

Figure 43: Study site 5, top: evening flight RGB, thermal, combination, VIS, NIR (figures 28,27,7,17,18) , and APEX classified (fig. 16); bottom: flight 1 RGB, thermal, combination, VIS, NIR (figures 30, 29, 9, 17, 18). The legends to the single images can be found at the original figure.

5.3.1 Position of typical Surface Structures

Lakes and deeply incised meltwater channels coincide with areas of cold ice (Ryser et al., 2013). These channels mostly have their accumulation area on the center of Grenzgletscher and tend to get bigger and deeper with length and more lateral position. The comparison of the images from 2016 and 2015 with the images from 2018 and 2019 only shows low displacement or movement within the shape of the deep channels.

Cryoconite holes are common among the whole central part of the cold ice, they have smaller sizes on ice ridges and get bigger in between the ridges due meltwater inflow. Cryoconite holes are getting less at the steeper sides. Because of downstream runoff impurities and cryoconite get transported by meltwater towards the glaciers margins or into bigger cryoconite sinks.

Moulins cannot be found on the lower ablation area, because they normally refreeze in cold ice (Ryser et al., 2013).

According to the classification results bright ice located in the center part of Grenzgletscher. Towards the side the ice gradually darkens.

Rocks and Debris is commonly found at side of the glacier tongue or close to the medial moraine.

6. Discussion

6.1 Classification

According to the classification results, the high spectral resolution and medium spatial resolution works good for classifying the surface of the ablation zone of Grenzgletscher. Also the coarser spectral and finer spatial resolution of the drone flight taken in 2019 produces good classification results. This raises the question of how few bands are needed for good classification results and what spectral ranges should be covered. The hyperspectral dataset of APEX can be used to produce typical spectral reflectance curves for glacier surface, which can be applied in supervised classification. The finer spatial resolution of the drone datasets aloud the detection of smaller surface structures, however the necessary of this must be evaluated. For modelling purposes the 2 m resolution seems perfectly suitable, since information about crevasses, melt water channels, supraglacial ponds and cold ice can be detected. Considering the size of the glacier and also of the different surface features it is questionable if smaller spatial resolution is really needed. Small scale surface structures on the Grenzgletscher are mostly Cryoconite holes and debris and rocks fallen onto the surface. It may be possible to characterize the composition of longitudinal surface structures, with a spatial resolution of 10 cm, otherwise these structures get mixed up with the surrounding surface.

Pope and Rees (2014.a) summarized other studies about glacier classification based on different spatial resolution and concluded, that there is no significant difference in measured glacier area using imagery at 60 m resolution of finer. They also mentioned that albedo variations is smaller than 30m pixels, but because albedo can vary within facies, which do not necessarily vary on the same scale. This can influence the surface classification with finer spatial resolution than 30 m, meaning that a surface class can be split up because of different albedo values. (Pope and Rees, 2014.a)

When looking at the acquisition time of the datasets from 2019 the question may be raised, why the flights were carried out in the late evening and early morning. This is especially the case, because multispectral imagery needs sunlight as light source. The mixture classes in the first and second morning flight may be due to the sunlight conditions. In the first morning flight parts of the valley side have been recorded too and especially the upper parts have been assigned to ice classes. But this region contains only bare soil, rock and some grass vegetation, which has a significant lower reflectance than ice, and should not be aggregated in the same class. This may be explainable due to the large height difference between the glacier surface and the valley site. The nearer position of the valley side to the drone may have increased the reflectance the sensor received from this area.

6.1.1 Spectral profiles of surface classes

The spectral profile of the APEX dataset show similar signatures with the profiles measured by Pope and Rees (2014.b). They found a typical peak at 1100 nm for glacier ice, which is also reported by many other studies, this peak can also be found in the APEX spectral profiles for ice classes. The multispectral drone do not show this peak, because their spectral range is limited to 470 – 875 nm. Snow and ice spectral typically show high reflectance from 350 - ~800 nm due to primary and multiple scattering (Pope and Rees, 2014.b). This high reflectance is found in all ice spectra produced in this thesis. Near infrared (~700 – 1400 nm) has been seen as containing quantitative information about snow and ice surfaces (Kokhanovsky and Zefe, 2004). This is also true for the APEX spectrum, the reflectance or the ice classes contained the peak at 1100 nm and then lower below the moraine classes. In the multispectral datasets only reaching till 875 nm the spectral profiles do not show any special features. Impurities on the snow surface lead to a darkening in the region of <900 nm (Warren and Wiscombe, 1980). The SWIR region (1450 – 2500 nm) can give information about on/off glacier (Casey et al., 2012).

When looking at the spectral profiles of the multispectral datasets, the region around 620 nm shows multiple peaks and lows, which cannot be found in the APEX spectrum. In this region the spectral range of the VIS camera (470 – 600 nm) and the NIR camera (600 – 875 nm) overlies. The NIR camera tend to record higher values than the VIS camera and therefore this up and downs in the spectrum were produced.

6.1.2 Findings and challenges

The discrimination between ice surface and moraine material is possible and also reliable for the classification with the APEX data as well with the multispectral data. However the APEX classification is may be more representative for the alation zone of Grenzgletscher and more useful for modelling purposes. Surface structures can be identified in all classifications, not as a separate class for crevasses or melt-water channels, but as been classified in a darker class within brighter classified surroundings. It needs to be mentioned, that the approach used in this thesis could not identify a separate water class, even when there is supraglacial run off and the presence of supraglacial lakes on the surface. This may be due to the shallow water or other factors, which must be further investigated.

The biggest challenge with the classification were the multispectral datasets from 2019. Since there were some problems arising in the processing, which lead to a spatial offset of different datasets covering the same area. This could possibly be avoided with a more careful processing and evaluation of the first outcomes.

When looking what kind of sensors are suggested to classify glacier surface the data from 2019 was not the best choice, since the spectral which is covered misses some distinguish features for glacier ice. But the results retrieved with the given data are generally acceptable for surface classification.

6.2 Thermal Images

Thermal data of glaciers is mainly collected within boreholes. In literature thermal imagery is not often used in context of glaciers. The main application of thermal imagery on glacier is for differentiating debris-covered glacier ice from debris next to the glacier.

6.2.1 Findings

The thermal images used in this thesis did generally represent the thermal distribution of the Grenzgletscher. The coldest areas in the thermal images were found among the center of the ablation area getting warmer towards the margins. This temperature distribution can be confirmed by borehole measurements (Ryser et al, 2013). The measured temperature values by the drones are biased, the image from 2016 is far to warm , while the images from 2019 recorded temperatures like those recorded from the accumulation area at Colle Gnifetti.

Thermal imagery allows the detection of debris covered ice within moraines, when there is only a thin debris-layer on the ice. This findings could be confirmed with the analysis of area of interest 1 in section (5.3.1).

During the study of the areas of interest the question arises, if classification could be done with a combination of RGB imagery and thermal imagery. Since most of the classification results would have been similar, when only classifying an RGB image. Especially when only two classes are asked.

6.2.2. Thermal Ghosts

Thermal ghost are features created by the mosaicking of single thermal images. They are mainly built on ice surface, since they do not appear in debris covered areas. Further investigation needs to be done on how the arising of these features can be eliminated or methods about how to remove those errors from the data. Therefore the last research question is answered. But it would be interesting to understand, why those features only occurred in the quite homogenous ice.

6.3 Surface Structures

Typical cold ice surface structures were found within areas of cold ice. At the start of this thesis, the aim was to somehow classify these structures. With unsupervised classification of multispectral data this could not be achieved. The classification worked for different ice classes according to their impurity. One of the goals was, to maybe classify cryoconite according their spectral features. This was mainly not possible due to the set up of the data, first of all the spatial was far to wide with 2 m for the APEX and 60-70 cm for the drone.

This thesis tired to connect surface structures with the cold ice body. There are some typically structures which are known to be indicators of cold ice, but structures which give indications about thermal changes in the glacier ice are more difficult to detect. The comparison of the 2016 shapes of deep channels to the images from 2019 only showed marginal changes. Therefore maybe cryoconite holes would be a better suitable surface structure to study. When with warmer ice temperature the viscosity of ice lowers then the ice should be more easily deformed by supraglacial run off. Meaning that the comparison of multispectral images collected multiple times during the melting season can give information, where the glacier surface is changing faster. This was not possible to do with only one dataset per year.

7. Conclusion

The classification of glacier surface into different two main classes (ice and moraine) and some subclasses based on the brightness could be successfully done by using multispectral or hyperspectral data. Classes representing bright or clean ice, which are typical for cold ice) were located in areas where cold ice was measured by Ryser et al. (2013). The classification were also mostly representative when only the VIS or NIR spectrum was included. The largest challenge of the multispectral classification are areas with debris-cover, but for bare ice the results are fine. However supraglacial water could not be classified within it's own class. Further studies can assess this challenge and maybe produce maps for meltwater on the glacier surface.

The thermal data can be used in analyzing the thermal distribution on the glacier surface. When comparing the thermal pattern of the evening image with morning and midday images effects of warming und cooling can be detected. Unfortunately the thermal data used in this thesis was only slightly overlaying so that this could not been deeper investigated. A diurnal dataset would be interesting to see, how temperature changes over a day. This could be used to analyze supraglacial meltwater and how it behaves over changing ice temperature.

Considering that the data used was biased and collected for a different purpose. The results are still meaningful and can help to better understand the surface the ablation zone of Grenzgletscher. The spectral profile generated with the APEX dataset can help by defining the right optical sensors for analyzing the Grenzgletscher. The APEX spectral profile covers a broad bandwidth and be used to validate other classifications.

8. References

APEX (2021). Airborne PRISM Experiment [online]. Available from: https://apex-esa.org/en/apex [Accessed 20.08.2021].

Benn, D. and Evans, D. (2010). Glaciers and Glaciation. Routledge, 2 Park Square, Milton Park, Abingdon, Oxon OX14 4RN.

Benoit, L., Aurélie, G., Raphaël, V., Inigo, I., Mathieu, G., Benjamin, L., Gunther, P., Dominik, G., Frederic, H., and Gregoire, M. (2018). A high-frequency and high-resolution image time series of the gornergletscher - swiss alps - derived from repeated UAV surveys.

Benson, C. S. (1960). Stratigraphic studies in the snow and firn of the Greenland ice sheet. (PhD). Pasadena, California: California Institute of Technology

Blatter, H. and Haeberli, W. (1984). Modelling temperature distribution in alpine glaciers. *Annals of Glaciology*. 5:18-22.

Blatter, H. and Hutter, K. (1991). Polythermal conditions in Arctic glaciers. *Journal of Glaciology*. 37(126):261-269.

Bolch, T., and Kamp, U. (2006). Glacier mapping in high mountains using DEMs, Landsat and ASTER data. Proceedings of the 8th international symposium on high mountain remote sensing cartography, 20–27 March 2005, La Paz, Bolivia.

Boon, S. and Sharp, M. (2003). The role of hydrologically-driven ice fracture in drainage system evolution on an arctic glacier. *Geophysical Research Letters*. 30(18):1916.

Brun, F., Dumont, M., Wagnon, P., Berthier, E., Azam, M. F., Shea, J. M., Sirguey, P., Rabatel, A., and Ramanathan, Al. (2015). Seasonal changes in surface albedo of Himalayan glaciers from MODIS data and links with the annual mass balance. *The Cryosphere.* 9:341–355

Casey, K.A., Kääb, A., and Benn, D.I. (2012). Geochemical characterization of supraglacial debris via in situ and optical remote sensing methods: A case study in Khumbu Himalaya, Nepal. *The Cryosphere*. 6(1):85–100.

Cuffey, K. M., & Patterson, W. S. B. (2010). The Physics of Glaciers (4th ed.)London: Academic Press.

Di Mauro, B., Baccolo, G., Garzonio, R., Giardino, C., Massabò, D., Piazzalunga, A., Rossini, M., and Colombo, R. (2017). Impact of impurities and cryoconite on the optical properties of the Morteratsch Glacier (Swiss Alps). *The Cryosphere*. 11:2393–2409.

8. References

Di Mauro, B., Garzonio, R., Baccolo, G., Franzetti, A., Pittino, F., Leoni, B., Remias, D., Colombo, R., and Rossini, M. (2020). Glacier algae foster ice-albedo feedback in the European Alps, *Scientific Reports.* 10:1–9.

Dumont, M., Brissaud, O., Picard, G., Schmitt, B., Gallet, J. -C., and Arnaud, Y. (2010). High-accuracy measurements of snow bidirectional reflectance distribution function at visible and nir wavelengths — Comparison with modelling results. *Atmospheric Chemistry and Physics*. 10(5):2507–2520.

Eisen, O., Bauder, A., Lüthi, M., Riesen, P., and Funk, M. (2009). Deducting the thermal structure in the tongue of Gornergletscher, Switzerland, from radar surveys and borehole measurements. *Annals of Glaciology*. 50(51):63-70.

Ewertowski, M.W., Evans, D.J.A., Roberts, D.H., Tomczyk, A.M., Ewertowski, W., and Pleksot, K. (2019). Quantification of historical landscape change on the foreland of a receding polythermal glacier, Hørbyebreen, Svalbard. *Geomorphology.* 325:40-54.

Ewertowski, M.W., and Tomczyk, A.M. (2020). Reactivation of temporarily stabilized ice-cored moraines in front of polythermal glaciers: Gravitational mass movements as the most important geomorphological agents for the redistribution of sediments (a case study from Ebbabreen and Ragnarbreen, Svalbard). *Geomorphology.* 350:106952.

Falconer, R.E., and Hogan, A.W. (1971). Capture of aerosol particles by ice crystals. Proc. Eastern Snow Conference.1–8.

Furfaro, R., Previti, A., Picca, P., Kargel, J.S., and Bishop, M.P. (2014). Radiative Transfer Modeling in the Cryosphere. Global Land Ice Measurements from Space, chapter 3. 53-73.

Gajda, R. (1958). Cryoconite phenomena on the greenland ice cap in the thule area. *The Canadian Geographer/Le Géographe Canadien*. 12.

Glasser, N.F. and Gudmundsson, G.H. (2012). Longitudinal surface structures (flowstripes) on Antarctic glaciers. *The Cryosphere*. 6:383-391.

Greuell, W. and de Wildt, M.D.R. (1999). Anisotropic reflection by melting glacier ice: Measurements and parametrizations in Landsat TM bands 2 and 4. *Remote Sensing of Environment.* 70:265–277-

Haeberli, W., and Funk, M. (1991). Borehole temperatures at the Colle Gnifetti core drilling site (Monte Rosa, Swiss Alps), *Journal of Glaciology.* 37(125):37–46

Haeberli, W., Huggel, C., Paul, F. and Zemp, M. (2021). The Response of Glaciers to Climate Change: Observations and Impacts. *Reference Module in Earth Systems and Environmental Sciences.* Treatise on Geomorphology (2013). 13:152-175.

Hagg, W., Hoelzle, M., Wagner, S., Mayr, E., and Klose, Z. (2013). Glacier and runoff changes in the Rukhk catchment, upper Amu-Darya basin until 2050. *Global and Planetary Change.* 110: 62–73.

Hartl, L., Felbauer, L., Schwaizer, G. and Fischer, A. (2020). Small-scale variability in bare-ice reflectance at Jamtalferner, Austria. *The Cryosphere.* 14:4063-4081.

Hendriks, J., Pellikka, P. and Peltoniemi, J. (2014). Estimation of anisotropic radiance from a glacier surface - Ground based spectrometer measurements and satellite-derived reflectances. University of Helsinki: Finnish Geodetic Institute.

Herzfeld, U.C., Clarke, G.K.C., Mayer, H., and Greve, R. (2004). Derivation of deformation characteristics in fast-moving glaciers. *Computers & Geosciences.* 30:291-302.

Huggel, C., Clague, J. J., and Korup, O. (2012). Is climate change responsible for changing landslide activity in high mountains? *Earth Surface Processes and Landforms.* 37(1):77–91.

Huss, M., A. Bauder, M. Werder, M. Funk, and R. Hock (2007). Glacier dammed lake outburst events of Gornersee, Switzerland. *Journal of Glaciology*. 53(181):189–200.

Huss, M., Hock, R., Bauder, A., and Funk, M. (2012). Conventional versus reference-surface mass balance, *Journal of Glaciology*. 58:278–286.

IPCC (2013). Climate Change 2013: The Physical Science Basis. Contribution of Working Group I to the Fifth Assessment Report of the Intergovernmental Panel on Climate Change. Authors: Vaughan, D.G., Comiso, J.C., Allison, I., Carrasco, J., Kaser, G., Kwok, R., Mote, P., Murray, T., Paul, F., Ren, J., Rignot, E., Solomina, O., Steffen, K., and Zhang, T.

Irvine-Fynn, T.D.L., Hodson, A.J., Moorman, I., Vatne, G., and Hubbard, A.L. (2011). Polythermal Glacier Hydrology: A Review. *Review of Geophysics.* 49:RG4002..

Karimi, N., Farokhnia, A., Karimi, L., Eftekhari, M., and Ghalkhani, H. (2012). Combining optical and thermal remote sensing data for mapping debris-covered glaciers (Alamkouh Glaciers, Iran). *Cold Regions Science and Technology.* 71:73-83.

Klok, E.J., Greuell, W., and Oerlemans, J. (2003). Temporal and spatial variation of the surface albedo of Morteratschgletscher, Switzerland, as derived from 12 Landsat images. *Journal of Glaciology.* 49(167):491–502.

Knap, W.H., Brock, B.W., Oerlemans, J., and Willis, I.C. (1999). Comparison of Landsat TM-derived and ground-based albedos of Haut Glacier d'Arolla, Switzerland. *International Journal of Remote Sensing.* 20:3293– 3310.

Kokhanovsky, A.A., and Zege, E.P. (2004). Scattering optics of snow. *Applied Optics*. 43(7):1589–1602.

Kraaijenbrink, P.D.A., Shea, J.M., Pellicciotti, F., de Jong, S.M., and Immerzeel, W.W. (2016). Object-based analysis of unmanned aerial vehicle imagery to map and characterise surface features on a debris-covered glacier. *Remote Sensing of Environment.* 186:581-595.

Lüthi, M. P., and Funk, M. (2001). Modelling heat flow in a cold, high altitude glacier: interpretation of measurements from Colle Gnifetti, Swiss Alps. *Journal of Glaciology*. 47(157):314–324.

Magono, C., Endoh, T., Ueno, F., Kubota, S., and Itasaka, M. (1979). Direct observations of aerosols attached to falling snow crystals. *Tellus*. 31(2):102–114.

Maisch, M., and Jost, D. (2006). Von der Eiszeit in die Heisszeit. Eine Zeitreise zu den Gletschern. Zytglogge Verlag. Oberhofen.

Naegeli, K., Damm, A., Huss, M., Schaepman, M., and Hoelzle, M. (2015). Imaging spectroscopy to assess the composition of ice surface materials and their impact on glacier mass balance. *Remote Sensing of Environment.* 168:388–402.

Naegeli, K. and Huss, M. (2017). Mass balance sensitivity of mountain glaciers to changes in bare-ice albedo. *Annals of Glaciology*. 58:119– 129.

Naegeli, K., Damm, A., Huss, M., Wulf, H., Schaepman, M., and Hoelzle, M. (2017). Cross-Comparison of albedo products for glacier surfaces derived from airborne and satellite (Sentinel 2 and Landsat 8) optical data. *Remote Sensing*. 9:110.

Naegeli, K., Huss, M., and Hoelzle, M. (2019). Change detection of bare ice albedo in the Swiss Alps. *The Cryosphere*. 13:397–412.

Nijhawan, R., Garg, P. and Thakur, P. (2016).

Ning, L., Xie, F., Gu, W., Xu, Y., Hunag, S., Yuan, S., Cui, W., and Levy, J. (2009). Using remote sensing to estimate sea ice thickness in Bohai Sea, China based on ice type. *International Journal of Remote Sensing.* 30(17):4539-4552.

Oeschger, H., Schotterer, U., Stauffer, B., Haeberli, W., and Rothlisberger, H. 1978. First results from Alpine core drilling ¨ projects. *Zeitschrift Gletscherkunde Glazialgeologie*. 13(1–2):193–208.

Painter, T.H. (2011). Comment on Singh and others, “Hyperspectral analysis of snow reflectance to understand the effects of contamination and grain size”. *Journal of Glaciology*. 57(201):183–185.

Paterson, W.S.B. (1994). The physics of glaciers. Third edition. Oxford, etc., Elsevier.

Paul, F., Barrand, N.E., Berthier, E., Bolch, T., Casey, K.A., Frey, H., et al. (2013). On the accuracy of glacier outlines derived from remote sensing data. *Annals of Glaciology,* 54(63):171–182.

Paul, F., Huggel, C., Kaab, A., (2004). Combining satellite multispectral image data and a digital elevation model for mapping debris-covered glaciers. *Remote Sensing of Environment.* 89:510–518.

Pellikka, P., and Rees, W. G. (2010). Remote Sensing of Glaciers. London: CRC Press.

Pettersson, R. (2004). Dynamics of the cold surface layer of polythermal Storglaciären, Sweden. Stockholm University. Stockholm.

Photonfocus (2021,a). Camera Series MV0-D2048x1088-C01-HS03-160-G2. *Product Guide.* Available from: https://www.photonfocus.com/products/camerafinder/camera/mv0-d2048x1088-c01-hs03-160-g2/ [Accessed 20.09.2021].

Photonfocus (2021,b). Camera Series MV0-D2048x1088-C01-HS02-160-G2. *Product Guide.* Available from: https://www.photonfocus.com/products/camerafinder/camera/mv0-d2048x1088-c01-hs02-160-g2/ [Accessed 20.09.2021].

Pope, E., and Rees, W. (2014,1). Impact of spatial, spectral, and radiometric properties of multispectral imagers on glacier surface classification. *Remote Sensing of Environment*. 141:1-13.

Pope, E., and Rees, W. (2014,2). Using in situ spectra to explore Landsat classification of glacier surfaces. *International Journal of Applied Earth Observation and Geoinformation*. 27:42-52.

Ranzi, R., Grossi, G., Iacovelli, L., and Taschner, S. (2004). Use of multispectral ASTER images for mapping debris-covered glaciers within the GLIMS project. IEEE transactions on geoscience and remote sensing symposium, 1144–1147.

Reinardy, B.T.I., Booth, A.D., Hughes, A.L.C., Boston, C.M., Åkesson, H., Bakke, J., Nesje, A., Giesen, R.H., and Pearce, D.M. (2019). Pervasive cold ice within a temperate glacier – implications for glacier thermal regimes, sediment transport and foreland geomorphology. *The Cryosphere*. 13:827-843.

Renaud, A. (1936). Les entonnoirs du glacier de Gorner. *Denkschriften der Schweizerischen Naturforschenden Gesellschaft*. 71(1):pp. 27.

Ryser, C. (2014). Cold ice in an alpine glacier and ice dynamics at the margin of the Greenland Ice Sheet. Mitteilungen 226, Versuchsanstalt für Wasserbau, Hydrologie und Glaziologie (VAW), R. M. Boes, Hrsg., ETH Zürich.

Ryser, C., Lüthi, M., Blindow, N., Suckro, S., Funk, M., and Bauder, A. (2013). Cold ice in the ablation zone: its relation to glacier hydrology and ice water content. *Journal of Geophysical Research: Earth Surface*. 118:693-705.

Scambos, T. A., Frezzotti, M., Haran, T., Bohlander, J., Lenaerts, J. T. M., Van den Broeke, M., et al. (2012). Extent of low-accumulation "wind glaze" areas on the East Antarctic plateau: Implications for continental ice mass balance. *Journal of Glaciology.* 58(210): 633–647.

Smiraglia, C., Maggi, V., Novo, A., Rossi, G., and Johnston, P. (2000). Preliminary results of two ice core drillings on Monte Rosa (Colle Gnifetti and Colle del Lys), Italian Alps. *Geografia Fisica e Dinamica Quaternaria*. 23(2), 165–172.

Sobota, I. (2011). Snow accumulation, melt, mass loss, and near-surface ice temperature structure of Irenebreen, Svalbard. *Polar Science.* 5:327-336.

Sold, L., Huss, M., Machguth, H., Joerg, P.C., Leysinger Vieli, G., Linsbauer, A., Salzmann, N., Zemp, M., and Hoelzle, M. (2016). Mass balance re-analysis of Findelengletscher, Switzerland; benefits of extensive snow accumulation measurements. *Frontiers in Earth Science*. 4.

Sugiyama, S., Bauder, A., Riesen, P., and Funk, M. (2010). Surface ice motion deviating towards margins during speed-up events at Gornergletscher, Switzerland. *Journal of Geophysical Research*. 115(F03010).

Suter, S., Laternser, M., Haeberli, W., Frauenfelder, R., and Hoelzle, M. (2001). First results from alpine core drilling projects. *Journal of Glaciology*. 47(156):85–96.

swisstopo (2021). Karten der Schweiz – Schweizerische Eidgenossenschaft [online]. Available from: https://map.geo.admin.ch [Accessed 15.01.2021].

Takeuchi, N. (2009). Temporal and spatial variations in spectral reflectance and characteristics of surface dust on Gulkana Glacier, Alaska Range. *Journal of Glaciology.* 55(192):701-709.

Thalmann, M. (2019). The Effect of Cold Ice on the Ablation of Grenzgletscher. University of Zurich. Zurich.

Warren, S.G. and Wiscombe, W. J. (1980). A model for the spectral albedo of snow. ii: Snow containing atmospheric aerosols. *Journal of the Atmospheric Sciences*. 37(12):2734–2745.

Werder, M.A., A. Loye, and Funk, M. (2009). Dye tracing a jökulhlaup: I. Subglacial water transit speed and water-storage mechanism. *Journal of Glaciology.* 55.:889–898.

Wientjes, I., and Oerlemans, J. (2010). An explanation for the dark region in the western melt zone of the greenland ice sheet. *Cryosphere.* 4:261268.

Wilson, N.J., Flowers, G.E., and Mingo, L. (2013). Comparison of thermal structure and evolution between neighboring subarctic glaciers. *Journal of Geophysical Research: Earth Surface*. 118:1443-1459.

Winther, J.-G. (1993). Landsat tm derived and in situ summer reflectance of glaciers in svalbard. *Polar Research*. 12(1):37–55.

Worni, R., Stoffel, M., Huggel, C., Volz, C., Casteller, A., and Luckman, B. (2012). Analysis and dynamic modeling of a moraine failure and glacier lake outburst flood at ventisquero negro, patagonian andes (argentina). *Journal of Hydrology*. 444-445:134–145.

Wu, Y., Wang, N., Li, Z., Chen, A., Guo, Z., and Qie, Y. (2019). The effect of thermal radiation from surrounding terrain on glacier surface temperatures retrieved from remote sensing data: A case study from Qiyi Glacier, China. *Remote Sensing of Environment.* 231:111267.

Zemp, M., Hoelzle, M., and Haeberli, W. (2009). Six decades of glacier mass-balance observations: a review of the worldwide monitoring network. *Annals of Glaciology*. 50:101–111.

9. Appendix

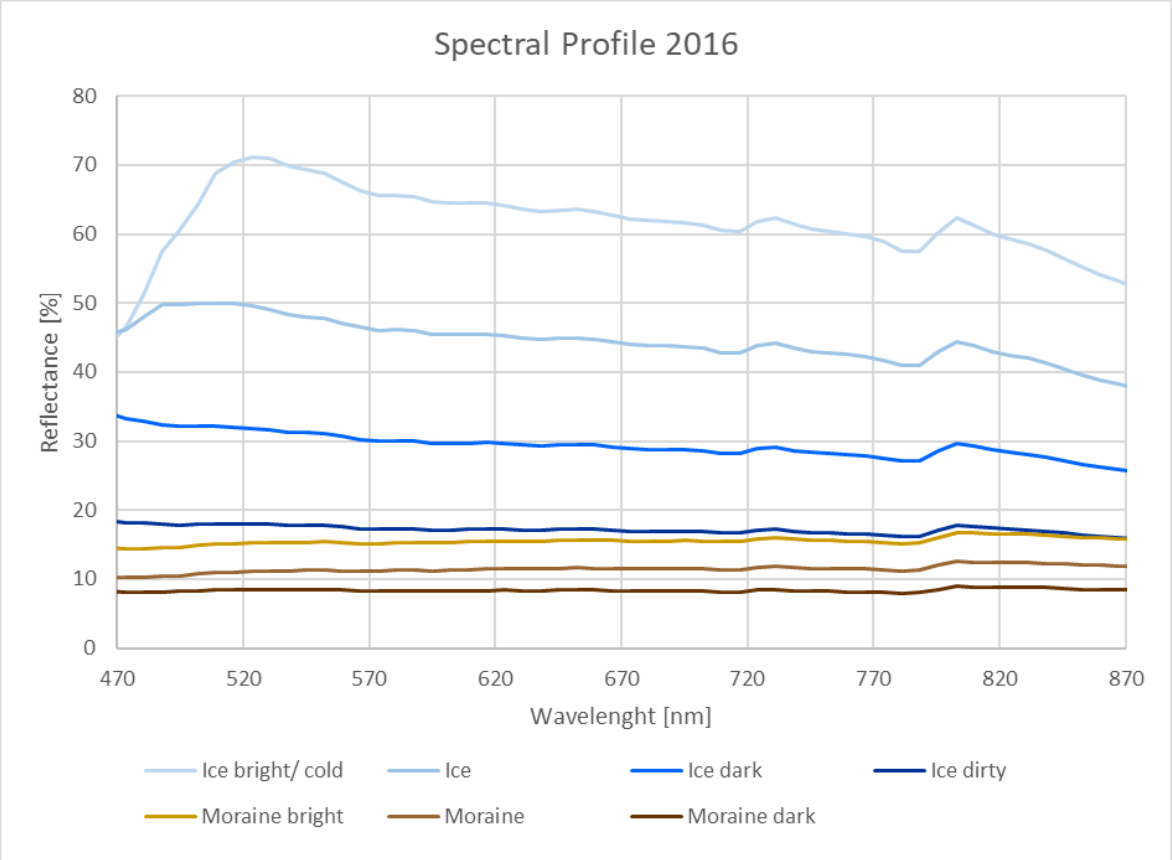

Figure 41: Spectral profile of the APEX classification stretched to the spectral range of the data from 2019.

10. Personal Declaration

I hereby declare that the submitted Thesis is the result of my own independent work. All external sources are explicitly acknowledged in this Thesis.

Zürich, 30.09.2021, Nicole Hanselmann